



Contents lists available at ScienceDirect

Physics Reports

journal homepage: www.elsevier.com/locate/physrep

Electronic properties of mesoscopic graphene structures: Charge confinement and control of spin and charge transport

A.V. Rozhkov^{a,b,*}, G. Giavaras^a, Yury P. Bliokh^{a,c}, Valentin Freilikher^{a,d}, Franco Nori^{a,e}

^a Advanced Science Institute, RIKEN, Wako-shi, Saitama, 351-0198, Japan

^b Institute for Theoretical and Applied Electrodynamics, Russian Academy of Sciences, 125412, Moscow, Russia

^c Department of Physics, Technion-Israel Institute of Technology, Haifa 32000, Israel

^d Department of Physics, Bar-Ilan University, Ramat-Gan 52900, Israel

^e Department of Physics, The University of Michigan, Ann Arbor, MI 48109-1040, USA

ARTICLE INFO

Article history:

Accepted 1 February 2011

Available online 22 February 2011

editor: D.L. Mills

Keywords:

Mesoscopic graphene structures

Nanoribbons

Quantum dots

pn-junctions

pnp-structures

Quantum barriers

ABSTRACT

This brief review discusses electronic properties of mesoscopic graphene-based structures. These allow controlling the confinement and transport of charge and spin; thus, they are of interest not only for fundamental research, but also for applications. The graphene-related topics covered here are: edges, nanoribbons, quantum dots, *pn*-junctions, *pnp*-structures, and quantum barriers and waveguides. This review is partly intended as a short introduction to graphene mesoscopics.

© 2011 Elsevier B.V. All rights reserved.

Contents

1. Introduction.....	78
2. Basic physics of a graphene sheet.....	78
3. Edges of graphene samples.....	80
3.1. Edge-stability issues.....	80
3.2. Electrons near edges.....	81
3.3. Graphene/graphane interface.....	83
3.4. Fabrication of high-quality edges.....	84
4. Graphene nanoribbons.....	84
4.1. Zigzag nanoribbons.....	84
4.1.1. Edge magnetism.....	84
4.1.2. Half-metallicity.....	86
4.2. Armchair nanoribbons.....	86
4.3. Nanoroads.....	87
4.4. Transport properties of nanoribbons.....	88
5. Quantum dots.....	89
5.1. Geometry-induced dots and graphene islands.....	90
5.2. Field-induced dots.....	93

* Corresponding author at: Advanced Science Institute, RIKEN, Wako-shi, Saitama, 351-0198, Japan.
E-mail address: arozhkov@gmail.com (A.V. Rozhkov).

5.3.	Nanoribbons of graphene and dots.....	95
5.4.	More dots	96
5.5.	Quantum rings	97
6.	Graphene <i>pn</i> -junctions and <i>pnp</i> -structures	97
6.1.	<i>pn</i> -junction.....	98
6.2.	Doping graphene by contact with metals	100
6.3.	<i>pnp</i> -structure	100
7.	Quantum barriers, wires, and waveguides.....	101
7.1.	Magnetic barriers: $B \neq 0, V = 0$	102
7.1.1.	Step-wise vector potential A : δ -function-like magnetic field B	102
7.1.2.	Step-wise magnetic field B : piece-wise linear vector potential A	102
7.2.	Combined magneto-electric barriers: $B \neq 0, V \neq 0$	103
7.3.	Waveguide with electrically-tuned parameters.....	104
8.	Conclusions.....	105
	Acknowledgements.....	107
	Appendix A. Tight-binding model of graphene lattice	107
	Appendix B. Edge states.....	108
B.1.	Armchair edge.....	108
B.2.	Zigzag edge.....	109
B.2.1.	Effect of the longer-range hopping.....	110
	References.....	110

1. Introduction

Graphene is a two-dimensional (2D) layer of carbon atoms ordered into a honeycomb lattice as shown in Fig. 1. It is a material with a host of unusual properties [1–10] including (among others): Dirac spectrum of low-lying quasiparticles [2], large mean-free-path [3], and high electron mobility [11,12].

Besides its purely fundamental importance, researchers view graphene as a promising new material for electronic [13], chemical [14], or electromechanical [15] applications, where graphene's unique properties may be of substantial benefit. Unlike 3D matter, whose bulk is hidden from direct observation and influence, graphene's "bulk", its 2D surface, is always exposed, and its structure may be inspected or modified with greater ease. Furthermore, the Dirac energy dispersion in 2D implies that graphene is a gapless semiconductor, whose density of states vanishes linearly when approaching the Fermi energy. As such, it is "a bridge material" separating the worlds of semiconductors (with an energy gap between the valence and conducting bands) and metals, with a finite density of electronic states at the Fermi energy. Depending on the operating regime, graphene can be pushed in either direction. For example, it is possible to open a gap in a sample with the help of chemical modifications [16,17], or lateral confinement [18–20]. Alternatively, one can make graphene metallic, e.g., by chemical doping [21]. Some graphene samples have spatially-varying electronic properties, due to local modifications on the sample. The long electronic mean-free-path, which can be of the order of micrometers, implies that electronic signals can travel unimpeded large distances through a device. These features might be very useful in applications.

The unusual properties of graphene motivated significant research efforts. The field grows very fast: the ISI web site reports that by October 2010 there were more than 5000 publications with the word "graphene" in their titles. Clearly, this is an enormous volume of scientific work, of which our brief review covers only a very small fraction. Its scope is very limited in several respects. As is obvious from the title, we direct our attention to mesoscopic graphene systems, a topic at the boundary between fundamental and applied research. Furthermore, we mainly discuss the electronic aspects of graphene mesoscopic systems, especially those which may be relevant for possible electronic or spintronic applications, for example, charge/spin transport and confinement, and control over them. Lattice properties are dealt with only when the lattice affects the electrons significantly. Several topics are deliberately omitted due to space constraints; these include: quantum Hall effect, thermal transport phenomena, phonons, and mechanical properties of graphene.

The review is organized as follows. In Section 2 we discuss the most basic electron properties of an infinite graphene sheet. The physics of graphene edges is reviewed in Section 3. Sections 4–6 focus on nanoribbons, quantum dots, as well as *pn*-junctions and *pnp*-structures, respectively. Section 7 discusses the barriers created by the combined application of magnetic and/or electric fields. Conclusions are presented in Section 8. The main part of the review is kept non-technical for it to be accessible by a general reader. More involved discussions are relegated to [Appendices](#).

2. Basic physics of a graphene sheet

For completeness, in this section we quickly remind the reader of the basic single-electron properties of a graphene sheet. A more detailed presentation can be found in [Appendix A](#). It is common to describe a graphene sample in terms of a tight-binding model on the honeycomb lattice. Lattice parameters for graphene, as well as some other microscopic characteristics,

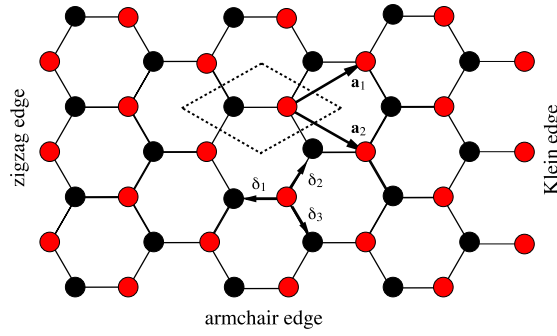


Fig. 1. (Color online) Geometry of the graphene lattice showing: primitive lattice vectors $\mathbf{a}_{1,2}$, diatomic lattice unit cell (dotted-line rhombus), and vectors $\delta_{1,2,3}$, connecting the nearest neighbors. Red (black) circles correspond to the \mathcal{A} (\mathcal{B}) sublattice. Three different types of edges (zigzag, armchair, and Klein edge) are shown. The Klein and zigzag edge violate the symmetry between the sublattices (the atoms at the edge sites belong exclusively to sublattice \mathcal{A} : they are all red), while the armchair edge does not (it has both black and red atoms).

Table 1

Graphene parameters at a glance.

Graphene parameters	Value
C–C bond length, a_0	1.4 Å
Lattice constant	2.46 Å
Hopping amplitudes:	
Nearest neighbor, t	2.8 eV
Next-nearest, t'	0.1 eV
Third-nearest, t''	0.07 eV
Fermi velocity, v_F	1.1×10^6 m/s

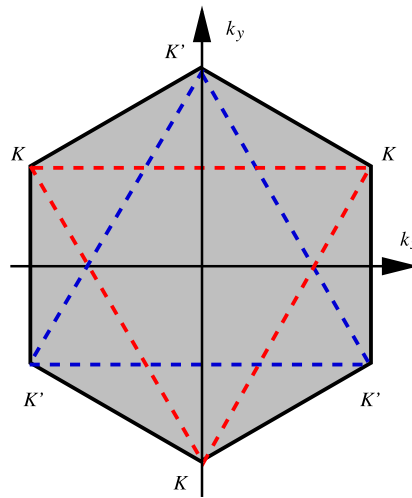


Fig. 2. (Color online) The Brillouin zone of graphene is a perfect hexagon. The Dirac cones are located at the corners of the Brillouin zone. The six cones can be split into two equivalence classes (cones within the same class are connected by dashed lines). These classes are commonly referred to as K and K' .

are given in Table 1. Honeycomb lattice can be split into two sublattices, denoted by \mathcal{A} and \mathcal{B} . The Hamiltonian of an electron hopping on a graphene sheet is given by

$$H = -t \sum_{\mathbf{R} \in \mathcal{A}} \sum_{i=1,2,3} c_{\mathbf{R}}^\dagger c_{\mathbf{R}+\delta_i} + \text{H.c.}, \quad (1)$$

where \mathbf{R} runs over sublattice \mathcal{A} , and $t = 2.8$ eV is the nearest-neighbor hopping amplitude. The vectors δ_i ($i = 1, 2, 3$) connect the nearest neighbors (see Fig. 1 showing the geometry of the graphene lattice). When necessary, H can be augmented by interaction or longer-range hopping terms (see Table 1 for values of the longer-range hopping amplitudes).

Since there are two atoms in graphene's unit cell, it is convenient to describe the single-electron wave function of graphene as a two-component spinor Ψ . This introduces an isospin quantum number. For every momentum \mathbf{k} lying within the Brillouin zone, Fig. 2, the Hamiltonian H has two eigenvalues $\varepsilon_{\mathbf{k}\pm}$, which have the same magnitude and opposite signs. The eigenvalue $\varepsilon_{\mathbf{k}+} > 0$ ($\varepsilon_{\mathbf{k}-} < 0$) corresponds to the conduction (valence) band of graphene.

The functions $\varepsilon_{\mathbf{k}\pm}$ vanish at the six corners of the Brillouin zone: $\mathbf{K}_{1,2} = (0, \pm 4\pi/(3\sqrt{3}a_0))$ and $\mathbf{K}_{3,4,5,6} = (\pm 2\pi/(3a_0), \pm 2\pi/(3\sqrt{3}a_0))$. Here the symbol a_0 denotes the carbon–carbon bond length. Near \mathbf{K}_i , $i = 1, \dots, 6$, the dispersion

Table 2

Brief summary of possible methods to induce an energy gap in monolayer and bilayer graphene. Asterisks (*) indicate experimental demonstrations; otherwise the value of the gap is a theoretical prediction. In some cases, the energy gap is tunable and its exact value critically depends on the details of the specific method. Here, 'BN-h' denotes boron nitride in the hexagonal configuration.

Inducing an energy gap in graphene		
Method	Gap in monolayer (meV)	Gap in bilayer (meV)
Nanoribbons* (width ~15 nm) [19]	200	
BN-h/Cu(111) substrate [27]	53/11	
SiC substrate* [28]	260	
External square superlattice [29]	65	
Strain engineering [22]	300	
Adsorption of molecules [30]	2×10^3	
Graphene covered by H ₂ O/NH ₃ [24]	18/11	30/42
Nanoribbons* (width ~30 nm) [31]		50
Electrical gates* [26]		250
Selective doping* (potassium) [25]		100
Electric field effect* [32]		150

surface can be approximated by two cones with a common apex

$$\varepsilon_{\mathbf{k}\pm} \propto \pm |\mathbf{k} - \mathbf{K}_i|. \quad (2)$$

The conduction and valence bands touch each other at the cones' apex.

Of the six cones only two can be chosen to be independent: the remaining four are connected to these two by a reciprocal lattice vector. Thus, the cones $\mathbf{K}_{1,\dots,6}$ can be split into two equivalence classes. These classes are commonly denoted by K and K' , and referred to as 'valleys'.

When graphene is not doped, its Fermi level passes through the cone apexes. In such a situation, if one is interested in the low-energy description, only the states near the cones must be accounted. For states with energies near the cone apexes, it is possible to use the following Weyl–Dirac equations

$$E\Psi_{1,2} = H\Psi_{1,2}, \quad (3)$$

$$H = -i\hbar v_F(\sigma_y \partial_x \mp \sigma_x \partial_y) = \hbar v_F \begin{pmatrix} 0 & -\partial_x \pm i\partial_y \\ \partial_x \pm i\partial_y & 0 \end{pmatrix}, \quad (4)$$

which have dispersion as in Eq. (2). These equations become invalid away from the cones. The spinor wave function Ψ_1 (Ψ_2) corresponds to the electron states near the cone K (K'). The upper (lower) sign in Eq. (4) corresponds to K (K'). The low-energy physics of electrons in graphene is equivalent to four species of two-dimensional massless Dirac electrons: two different spin directions and two cones, K and K' , giving overall fourfold degeneracy.

Pristine undoped graphene is a gapless semiconductor. This means that its density of states does not have a gap, but vanishes linearly when the energy approaches the apexes. Sometimes it is desirable to open a gap in the graphene spectrum. As shown in Table 2 this can be achieved by employing various mechanical, electronic, and/or chemical methods. In particular, in monolayer graphene the gap can be induced by substrate or strain engineering [22,23], as well as by deposition or adsorption of molecules on the graphene layer, such as, for example, water and ammonia [24]. Based on numerical studies, the value of the energy gap can range from a few meV to hundreds of meV. Most importantly it can be larger than room temperature as required for graphene-based transistors. In bilayer graphene the gap can be induced and continuously tuned, for instance, chemically through selective doping [25], or even electrically by applying gate voltages [26]. The fact that graphene's band structure can be controlled externally and with rather simple processes is a nontrivial result which reveals the potential of graphene for nanotechnology.

3. Edges of graphene samples

The characteristics of a mesoscopic device depend substantially on its edges. Therefore, it is important to study the electron behavior near the graphene edge.

3.1. Edge-stability issues

Two kinds of edges are often discussed in the literature: zigzag and armchair. A form of the zigzag is the Klein edge [33]. All three types are shown in Fig. 1. They are the most symmetric variants of edges in graphene. More complicated edges were also studied [34–38].

Of course, in a laboratory sample some of these edge types may be unstable chemically or undergo reconstruction. The possibility of the edge reconstruction has been addressed in several publications. Most importantly, it appears that the pristine zigzag edge is unstable: recently, it was predicted on the basis of density-functional theory (DFT) calculations [39] that it might undergo reconstruction at room temperature, and become a *reczag* (short for 'reconstructed zigzag' [40]), see



Fig. 3. Reczag, or ZZ 57, edge of a graphene sheet, from Ref. [39]. In the right panel the edge unit cell is shown. It consists of a pentagon and a heptagon. The latter polygons are the reason why this edge type is called '57'. Numbers in the right panel are the bond lengths in Å. Source: Reprinted figure with permission from P. Koskinen, S. Malola, and H. Hakkinen, Phys. Rev. Lett. **101**, 115502 (2008). © 2008, by the American Physical Society.

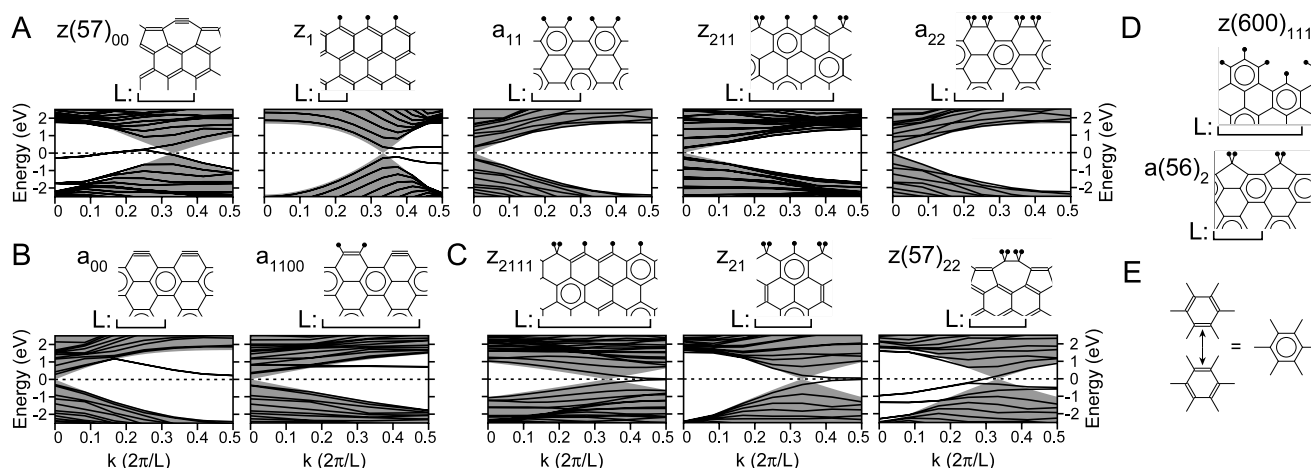


Fig. 4. Stable types of graphene edges, from Ref. [41]. Row A of the figure shows the five most stable configurations of the graphene edge with and without hydrogen attached to the unsaturated bonds. There, hydrogen is represented by small black circles. Rows B and C show other stable armchair and zigzag terminations. The DFT calculations reported in Ref. [41] predict that monohydrogenated zigzag denoted as z_1 in the figure and reczag denoted as $z(57)_{00}$ are stable only at extremely low hydrogen concentrations. At standard atmospheric conditions, a_{11} , z_{211} , and a_{22} are the most stable types of edges. Note that the pristine zigzag edge (studied in numerous papers) is *not* listed as a stable configuration. More complicated types of the graphene terminations are presented in panel D. In panel E the representation of the benzenoid aromatic carbon ring as a superposition of two degenerate Kekule configurations is shown.

Source: Reprinted figure with permission from T. Wassmann, A.P. Seitsonen, A.M. Saitta, M. Lazzeri, and F. Mauri, Phys. Rev. Lett. **101**, 096402 (2008). © 2008, by the American Physical Society.

Fig. 3). This kind of edge is often called 'ZZ 57'; namely, it is a version of zigzag (thus ZZ) edge, in which the edge hexagons are replaced by pentagons and heptagons (hence the 5 and 7). Experimental data supporting the existence of the reczag edge were presented in [40]. A similar conclusion was reached in [38]: the energy of the zigzag edge is substantially higher than the energy of the reczag. In Refs. [41,42] the non-hydrogenated zigzag edge was not listed among stable configurations.

The conclusions of Ref. [39], regarding the relative stability of zigzag and reczag, were challenged in Ref. [43], where the experiment of Ref. [44], proving the existence of the zigzag edge in a laboratory sample, was quoted. The experimental demonstration of the zigzag edge stability was also reported in Ref. [45]. Results of Ref. [46] are also in disagreement with Ref. [39]. However, the authors of Ref. [46] were unsure whether their molecular dynamics simulations can provide a reliable answer to the question of the edge stability.

The chemical stability was also investigated. It was pointed out in Refs. [41,42] on the basis of DFT calculations that the reczag and armchair are stable only when the concentration of hydrogen in the surrounding media is very small. If this is not the case, other types of edges, with hydrogen atoms attached, are stabilized (see Fig. 4). The results of DFT are consistent with Clar's theory of the aromatic sextet [47,48].

The DFT calculations of Ref. [38] demonstrated that the energy of zigzag, armchair, reczag, and more complicated regular edges always decreases upon monohydrogenation. This agrees with Ref. [41]: when enough hydrogen is present in the surrounding media, hydrogenation of the edge occurs.

These results suggest that the edge stability is a complicated problem in graphene. The edge stability depends on the orientation of the edge and is affected by the chemical environment (see Table 3).

3.2. Electrons near edges

The simplest way to describe an electron near the edge is to resort to the Weyl–Dirac equation (3) with appropriate boundary conditions. One has to keep in mind that the realistic boundary condition depends on a variety of factors: the orientation of the edge, deformation of the chemical bonds near the edge, edge reconstruction, and possible chemical functionalization of the unsaturated bonds. Theoretical studies of these conditions were performed in several papers [34,36,50–52].

Table 3

Different properties of graphene edges. In addition to the three types presented in Fig. 1 (zigzag, armchair, and Klein edges), a *reconstructed zigzag* (reczag) edge [40] is now included in this comparison.

Graphene edges				
	Zigzag	Armchair	Klein	Reczag
Stability [39]	Unstable (to reczag)	Stable		Stable
Edge states	Yes	No	Yes	
Magnetism [41]	Ferromagnetic	No		No
Stress [49]	Compression	Compression		Tension (weak)

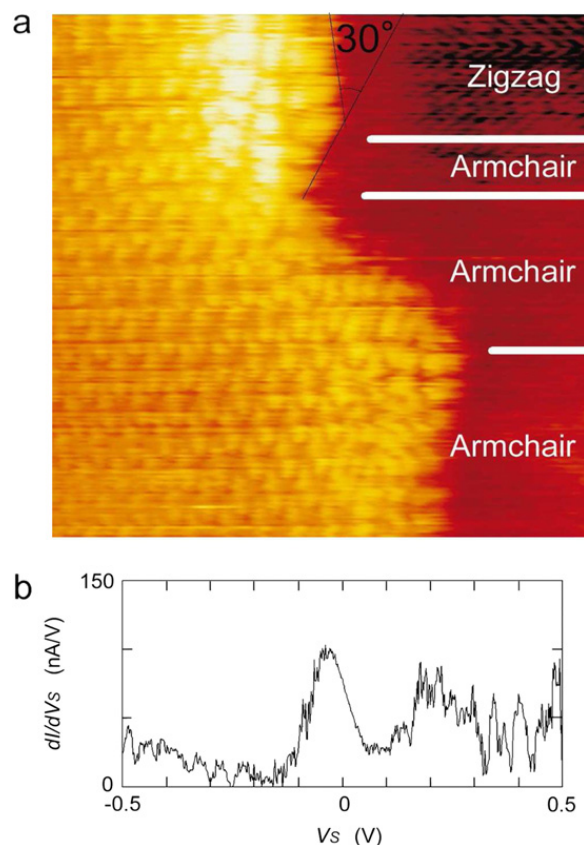


Fig. 5. (Color online) Scanning tunneling microscope image of different graphene terminations, from Ref. [54]. (a) The termination of a graphene sample is investigated using a scanning tunneling microscope. Fragments of both zigzag and armchair types are identified. The edge states near the zigzag edge are clearly visible as stripes of bright spots stretching along the zigzag edge. No edge states are present near the armchair termination. (b) A typical dependence of the differential conductance near the zigzag edge is plotted. The peak near the zero voltage ($V_s = 0$) corresponds to the edge states.

Source: Reprinted figure with permission from Y. Kobayashi, K.-i. Fukui, T. Enoki, K. Kusakabe, and Y. Kaburagi, Phys. Rev. B **71**, 193406 (2005). © 2005, by the American Physical Society.

The physics of electrons near the armchair edge is simple: the edge always acts as a reflector of the incident electron current. The scattering is affected by details of the edge structure, such as C–C bond lengths near the edge and non-carbon radicals attached to the edge. Some additional details are provided in Appendix B.1.

The physics of Klein and zigzag edges, however, is quite different. These edges bind electrons. When the nearest-neighbor hopping Hamiltonian is used to describe graphene, the bound eigenstates (edge states) form a dispersionless band at the zero of energy (see Appendix B.2). These edge states can be observed experimentally as a peak in the local density of states [44,53,54]. For example, Fig. 5 shows scanning tunneling microscopy data from Ref. [54]. There, the edge states are seen near the zigzag edge as a stripe of bright spots extending along the edge.

The dispersionless band of the bound states is unstable with respect to different perturbations of H . For example, the inclusion of longer-range hopping makes the band disperse (Refs. [51,52,55–58] and Appendix B.2).

The most interesting way of lifting the degeneracy of edge states is by adding electron–electron interactions to H . It was predicted quite some time ago [59] that magnetic correlations develop at a zigzag edge as a result of the interaction. This effect was investigated in several papers [60–63]

For example, a detailed DFT study was reported in Ref. [60]. It predicts that an isolated graphene zigzag edge is a ferromagnet with magnetic moment m of 0.3 of the Bohr magneton per unit cell of the zigzag edge. This may be understood qualitatively as follows. The spin coupling between nearest-neighbor carbon atoms is antiferromagnetic. Thus, different

Table 4

Summary of the magnetic properties of the graphene zigzag edge, as reported in Ref. [60]. When the electron–electron interaction is taken into consideration, the edge-state degeneracy is lifted through the magnetization of the electrons near the edge. This creates a one-dimensional magnetic system. The magnetic momentum M of such system is 0.3 of the Bohr's magneton per zigzag edge unit cell. The correlation length ξ at room temperature is rather short, suggesting that it would be difficult to utilize the pristine zigzag edge in a spintronic device operating at room temperature. However, below $T_x = 10$ K, a crossover to Ising-like magnetic correlations occurs, and the correlation length increases exponentially upon approaching $T = 0$. It was proposed [60] that ξ could be as large as a micrometer.

Zigzag edge magnetism			
M per unit cell	$\xi(T)$ $T = 300$ K	$\xi(T)$ $T < 10$ K	Anisotropy
$0.3 \mu_B$	~ 1 nm	$\sim 1 \mu\text{m}$	Ising, 10^{-4}

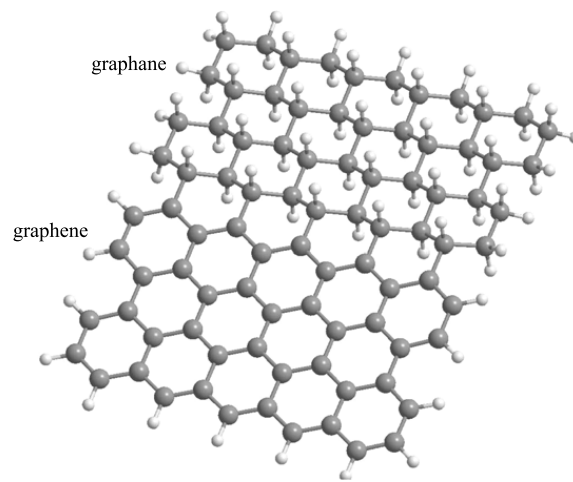


Fig. 6. Graphene/graphane interface, as studied in Ref. [66]. Larger dark balls correspond to carbon atoms, while the smaller light balls correspond to hydrogen. The lower part of the sample that is shown is graphene, while the higher part is graphane. In bulk graphane every carbon atom has a hydrogen atom attached to it.

sublattices have opposite magnetic momenta. In the bulk, this would lead to cancellation of the total moment. Near the edge, however, the electron density at the exposed row is higher than at rows located deeper into the bulk. Most importantly, all sites at the zigzag edge belong to the same sublattice; therefore, they have the same magnetic moment. This leads to a local imbalance of the total magnetic moment, which is seen as edge ferromagnetism.

Ref. [60] reports many properties of the edge ferromagnetism (see also Table 4): spin-wave dispersion ($E = \kappa q^2$, where $\kappa = 320 \text{ meV \AA}^2$), stiffness ($D = 2\kappa/m = 2100 \text{ meV \AA}^2$), magnetic anisotropy ($\sim 10^{-4}$), and crossover temperature between the Heisenberg and the Ising regimes ($T_x \sim 10$ K). The spin correlation length at room temperature is estimated to be of the order of one nanometer. At temperatures below T_x it increases exponentially as the temperature decreases. The effects of edge disorder on the magnetic properties of the zigzag edge were also investigated.

In Ref. [61] magnetic properties of small fragments of zigzag edge were studied using the Hubbard model. Such model is relevant for systems with rough edges, consisting of alternating fragments of different terminations. It was demonstrated that a very short, of the order of three lattice constants, zigzag sequence is sufficient to generate a local magnetic moment.

Some other interacting effects have also been studied. For example, the influence of the long-range Coulomb interaction and doping on the edge magnetism was discussed in Ref. [63] using the Hubbard model with Coulomb interactions. The interaction of edge states with phonons was studied in Ref. [64].

3.3. Graphene/graphane interface

Graphane [17,65] is a hydrogenated sheet of graphene. Unlike graphene, graphane is a semiconductor with a gap of the order of few eVs. The graphene/graphane interface, shown in Fig. 6, can be viewed as a type of graphene edge: low-lying electron states in graphane decay exponentially inside the gapped media of graphane. As demonstrated by molecular dynamics simulations [66], the interface remains almost atomically sharp even at sufficiently high temperatures, which is an extremely attractive feature since it reduces scattering and simplifies the theoretical description.

Depending on the orientation of the interface relative to the crystallographic axis of graphene, one can distinguish a zigzag-type interface (as in Fig. 6), or an armchair-type (at the right angle to the zigzag). The zigzag interface supports edge states whose electronic and magnetic properties were investigated in Ref. [67].

Besides hydrogenation, graphene may be subjected to fluorination in order to produce fluorinated graphene [68–72]. Like graphene, the latter is a semiconductor with a gap of the order of a few eV. A similar conversion occurs upon functionalization of graphene by nitrophenyl [73]. The properties of the interface between pure graphene and the functionalized material must be similar to the properties of the graphene/graphene interface.

3.4. Fabrication of high-quality edges

Most of the theoretical work so far has assumed that the edges of the nanostructures are atomically perfect. Needless to say, this is not easy to realize experimentally. However, recently, substantial progress in the area of high-quality edge fabrication has been achieved (e.g., [74,75]).

In Ref. [74] a chemical method of deriving narrow graphene stripes with sharp edges was reported. A graphene sample was placed in a solvent and subjected to sonification. Strips with sharp edges and widths varying from 50 nm to sub-10 nm were extracted from the solution. The strips produced were used to fabricate a field-effect transistor-like device.

In Ref. [75] it was experimentally demonstrated that during Joule heating of the graphene sample with disordered edges carbon atoms at the edge were vaporized, and sharp edges were stabilized. Model calculations showed that the edge defects were healed through point defect annealing and edge reconstruction. This process was modeled in Ref. [76]. These findings suggest that many theoretical predictions dependent on the edge quality could be tested experimentally.

4. Graphene nanoribbons

Nanoribbons, which are strips of graphene, are among the most studied mesoscopic graphene structures. There are several reasons for this. First, they demonstrate unusual physical properties, for example, edge states, which might be used in future spintronics applications. Second, nanoribbons are easy to produce and demonstrate excellent transport properties.

Third, they have an energy gap in their single-electron spectrum. This gap is a consequence of the electron confinement, and it is inversely proportional to the width of a nanoribbon [19,20]. This suggests that, at least in principle, a nanoribbon with a desired value of the gap may be fabricated. Finite gap and high mobility are both very useful for the design of field-effect transistors (FET): they allow for large on/off ratios, small losses, and high operating frequencies. For example, a nanoribbon-based FET realized in Ref. [77] demonstrated an on/off ratio of about 10^6 at room temperature. Other nanoribbon-FET devices were described in Refs. [78,79]. (Carbon nanotubes also have a gapped spectrum. However, their fabrication process is much more involved).

Nanoribbons are usually classified by their type of edge; for instance, there are zigzag and armchair nanoribbons. Nanoribbons may also have disordered [7] or more complicated regular types of edges [80].

4.1. Zigzag nanoribbons

Many interesting properties of zigzag nanoribbons are related to the presence of edge states in the nanoribbon electron spectrum. These states may be derived, together with other low-lying states, with the help of Eq. (3) supplemented by a boundary condition suitable for the zigzag edge [81]. The resultant spectrum is shown in Fig. 7(a). Two almost dispersionless branches connecting the Dirac cones, K and K' , correspond to the edge states. They are analogous to the edge states discussed in Section 3.

Similar conclusions about edge states may be reached using first-principle calculations. These reveal that the zigzag nanoribbon is a semiconductor with a width-dependent gap [82–84]. The lowest energy states are edge states.

4.1.1. Edge magnetism

Edge states are responsible for magnetism in zigzag nanoribbons. Edge magnetism is an interesting feature with potential spintronic applications; since the edge-state branch is both magnetized and able to carry current, it can be used to couple spin magnetization and current. This property may be used to control the magnetization with current or vice versa.

The magnetism of a nanoribbon with pristine zigzag edges was investigated theoretically in 1996 [91]. It is quite similar to the magnetism of an isolated zigzag edge: each edge of the nanoribbon has a finite magnetization, which is induced due to the instability of a nearly-flat edge-state band. There is a non-zero coupling between the magnetizations of the two edges. In Ref. [91] it was shown that this coupling is antiferromagnetic, i.e., the magnetization vectors at the opposite edges are antiparallel. Such result is easy to understand. Consider the following two statements: (i) repulsive interactions between electrons on a half-filled bipartite lattice induce an antiferromagnetic correlation between sublattices; (ii) in case of the zigzag nanoribbon, one of its edges always terminates in atoms of \mathcal{A} sublattice, the opposite edge terminates in atoms of \mathcal{B} . As a consequence of (i) and (ii), the local antiferromagnetic tendency is translated into weak inter-edge antiferromagnetic interactions.

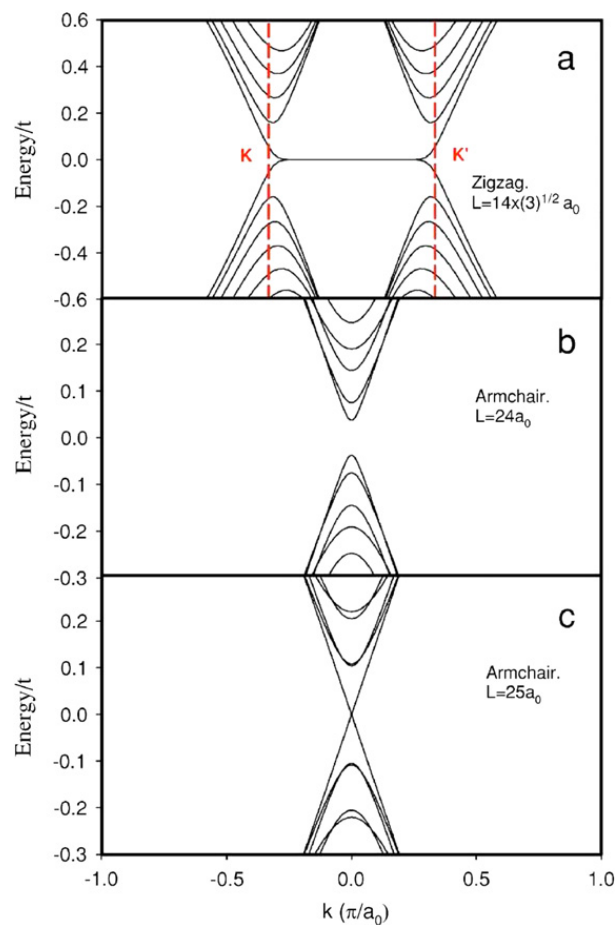


Fig. 7. (Color online) Single-electron energy spectrum of a nanoribbon calculated with the help of the Weyl–Dirac equation (3), from Ref. [81]. Due to the finite width of a nanoribbon, the transverse momentum is quantized. Therefore, the nanoribbon’s spectrum consists of a number of branches corresponding to different values of the quantized momentum. Since the graphene lattice is anisotropic, the spectrum of a zigzag nanoribbon [panel (a)] differs in several respects from the spectrum of an armchair nanoribbon [panels (b) and (c)]. For the zigzag nanoribbon the remnants of two Dirac cones, K and K' , are visible. The almost flat branch connecting K and K' corresponds to the edge states. It acquires a very weak dispersion due to interference of the edge states (exponentially) localized at the opposite edges of the nanoribbon. For the armchair nanoribbon both K and K' ‘coalesce’ together. According to the calculations of Ref. [81], the armchair nanoribbon may be either a semiconductor with a small gap [panel (b)], or a gapless metal [panel (c)]. The size of the gap depends on the nanoribbon’s width. However, more elaborate treatments accounting for the electron–electron interaction [85,86], electron–lattice interaction [18,87,88], or longer-range hopping [89,90] proved that the gap is always non-zero.

Source: Reprinted figure with permission from L. Brey and H. Fertig, Phys. Rev. B **73**, 235411 (2006).

© 2006, by the American Physical Society.

Since the pristine zigzag edge is likely to be chemically unstable [41,42], it is therefore important to study nanoribbons with non-carbon atoms or functional groups attached to the edges. The case of a zigzag nanoribbon with monohydrogenated edges was discussed in Ref. [83]. Such nanoribbons support edge states and have an edge ferromagnetic moment with antiferromagnetic coupling between the edges. This is consistent with the results of Ref. [41], where an extensive list of various edge types and their properties was presented. However, not all versions of functionalized or reconstructed zigzag edge support magnetism.

A chemical way to produce a nanoribbon with finite magnetic moment was proposed in Ref. [92]: since the opposite edges of the zigzag nanoribbon have opposite magnetic momenta, a disparity (e.g., a non-equivalent chemical functionalization) between the two edges may create a nanoribbon with non-zero magnetization. Local-spin-density calculations reported in Ref. [92] proved that fact for the nanoribbon whose one edge is monohydrogenated, while the other is the dihydrogenated (see Fig. 8). This result can be easily understood qualitatively. The monohydrogenated edge is ferromagnetic, while the dihydrogenated is non-magnetic [41]. Thus, the whole system is ferromagnetic.

Ref. [93] presented a very detailed DFT study of the effect the edge functionalization exerts on the zigzag nanoribbon’s magnetism. The main focus there was the monohydrogenated zigzag nanoribbon, where some of the hydrogen atoms were replaced by other radicals. When the edges have non-identical chemical structure (i.e., one edge is purely hydrogenated, the other has some of its hydrogens substituted), it was determined that a finite magnetization may be generated. The

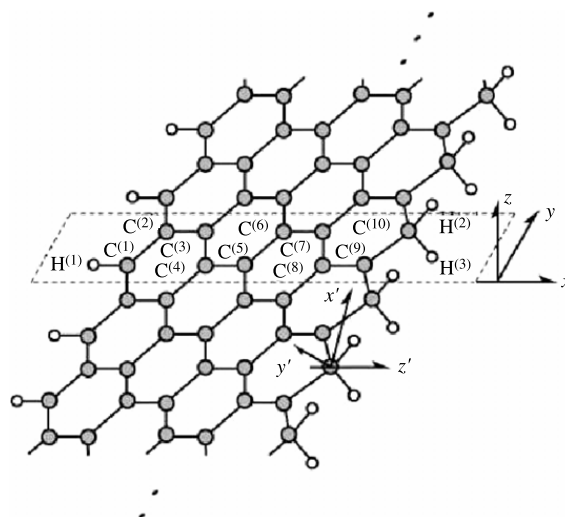


Fig. 8. Zigzag nanoribbon with disparity between edges, from Ref. [92]. The nanoribbon edges are parallel to y -axis. The left edge is monohydrogenated, while the right edge is dihydrogenated. Here, filled circles are carbon atoms, empty circles are hydrogen atoms. Since the opposite edges of a pristine zigzag nanoribbon have opposite magnetic momenta, a disparity between the two edges may induce a non-zero magnetization of the nanoribbon. Indeed, a local-spin-density approximation study [92] revealed that the nanoribbon in the figure possesses a finite magnetic moment. This result can be easily understood qualitatively. The monohydrogenated edge is ferromagnetic, while the dihydrogenated is non-magnetic. Thus, the whole system is ferromagnetic.

Source: Reprinted figure with permission from K. Kusakabe and M. Maruyama, Phys. Rev. B **67**, 092406 (2003).

© 2003, by the American Physical Society.

effect is particularly strong for the oxygen substitution. This result is consistent with Ref. [92]. It was also reported that such nanoribbon has different band gaps for different spin orientations. This state can be described as a spin-selective semiconductor.

In addition, it was shown in Ref. [93] that not only the magnetic properties but the band gap of a zigzag nanoribbon is sensitive to the chemical functionalization of the edges as well. For example, doping with oxygen may close the gap, provided that oxygen concentration is sufficiently high. A variety of other effects dependent on the edge chemistry was also discussed.

4.1.2. Half-metallicity

A half-metal is a conductor whose charge carriers are fully spin-polarized. This is a very desirable property with potential applications to spintronics because it can be used to create a fully spin-polarized current. Ref. [82] suggested that the application of a transverse electric field to a zigzag nanoribbon closes the gap for one spin orientation. The gap for another spin orientation is increased even more (see Fig. 9). A similar conclusion was reached in Ref. [94]. Note that this idea is also based on inducing a disparity between the two edges: this time the transverse field is the agent producing the disparity.

The proposal [82] summarized in the previous paragraph was disputed in Ref. [95], where it was argued that, when the transverse field is applied, the gap values for the spin-up and the spin-down electrons are different. However, both gaps are finite for any value of the electric field, producing a spin-selective semiconductor, and not half-metal. Ref. [95] attributed the discrepancy to the artifacts of the computational technique of Ref. [82].

A suitable functionalization can enhance the half-metallic features of the zigzag nanoribbon [96]. Also, Ref. [97] explored a wider range of chemical modifications of zigzag nanoribbons in search for robust half-metallicity. The results in Ref. [96,97] suggested that the chemical modifications may be a powerful tool for the control of the zigzag nanoribbon's half-metallic properties.

4.2. Armchair nanoribbons

The electron properties of the armchair nanoribbon are simpler than those of the zigzag nanoribbon. Both tight-binding model and Weyl–Dirac equation calculations show that graphene armchair nanoribbons with pristine edges may be either in a semiconducting (finite gap, Fig. 7(b)), or metallic (zero gap, Fig. 7(c)), state with the gap oscillating as a function of the nanoribbon's width. A more accurate numerical study [18] from 1997, which allowed for deformation of the carbon–carbon bonds dangling at the edges, proved that the metallic state is unstable: the dangling bonds deform, inducing a finite gap in the electron spectrum. Thus, according to Ref. [18], the armchair nanoribbon is always a semiconductor (see Fig. 10).

The above line of reasoning was generalized in Ref. [88], where it was shown analytically that the metallic state of an armchair nanoribbon is generically unstable: the edge bond instability is only one possibility. It was also discussed [88] how the electron gap of a *finite-length* armchair nanoribbon can be effectively closed with the help of chemical modifications of the nanoribbon's edge.

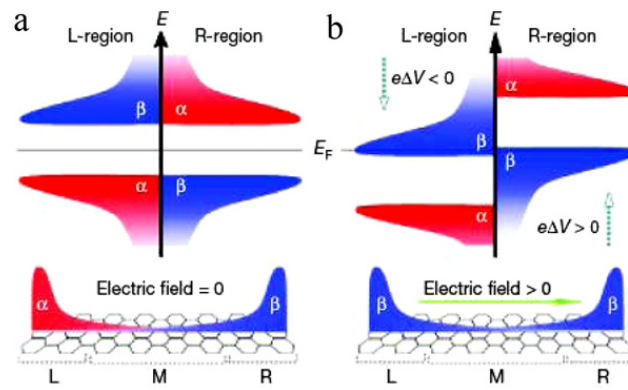


Fig. 9. Zigzag nanoribbon without (a) and with (b) a transverse electric field, from Ref.[82]. Symbols α (β), in red (blue), represent the spin-up (spin-down) orientations of the edge band electrons. In the lower part of panel (a) both orientations are present: spin-up is on the left edge (L) of the nanoribbon, and spin-down is on the right edge (R). The letter 'M' stands for 'middle' of the nanoribbon. In the upper part of (a) the energies of different edge states are plotted. On the left edge, the spin-up states are filled ($E < 0$), and the spin-down are empty. On the right edge, the situation is reversed. Panel (b) shows what happens when a transverse electric field is applied. The electrostatic potential pushes down the states on the left edge, and pushes up the states on the right edge. As a result, the density of states at the Fermi energy is zero (finite) for spin-up (spin-down) electrons. The system becomes half-metal: it is a conductor (metal), since there is a finite density of current-carrying states at the Fermi energy, yet, these states correspond only to one spin polarization (spin-down).

Source: Reprinted by permission from Y.-W. Son, M.L. Cohen, and S.G. Louie, Nature **444**, 347 (2006).
 © 2006, by Macmillan Publishers Ltd: Nature.

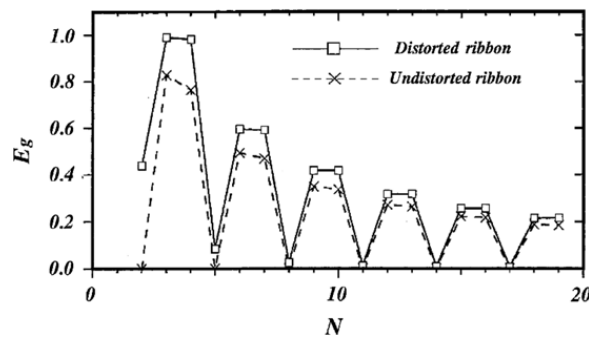


Fig. 10. Armchair nanoribbon's gap as a function of the nanoribbon's width, from Ref. [18]. The tight-binding calculation (dashed line) predicts that the gap of the armchair nanoribbon vanishes periodically as a function of the nanoribbon's width. However, the numerical calculations within a more elaborate model, which allows for deformation of the carbon–carbon bonds, prove that the gap is non-zero (albeit very close to it) for any width (solid line), although, the dependence on the width remains oscillatory. An analytical demonstration of the instability of the zero-gap state is given in Ref. [88]. This instability occurs because the increase of the elastic energy due to the lattice deformation is smaller than the decrease of the electron kinetic energy due to the gap opening.

Source: Figure is reprinted from: M. Fujita, M. Igami, and K. Nakada, J. Phys. Soc. Jpn. **66**, 1864 (1997).

A gap may also be generated by electron–electron interactions [85], or longer-range hopping [89,90]. In several papers, the electronic gap was determined with the help of first-principles techniques. Refs. [80,87] reported DFT calculations of the gap for the armchair nanoribbon with different widths, with both pristine and monohydrogenated armchair edges. The results of Ref. [80] for the gap are summarized in Table 5. Refs. [19,20] reported the experimental measurement of the gap. The experimental value for the gap was found to be consistent with the results of DFT calculations. However, Ref. [84] claimed that DFT underestimates the gap, and the use of the so-called GW approximation [98] is more appropriate. GW values of the gap are significantly higher than DFT values.

The effect of the edge functionalization on the spectral gap was studied in Ref. [93]. The gap was found to be robust against functionalization. This is different from the case of zigzag nanoribbons whose gap is very sensitive to the chemical structure of the edges (see Section 4.1).

Thus, it is expected on the basis of theoretical studies that an armchair nanoribbon is a semiconductor with a width-dependent gap, whose value is rather insensitive to the edge's chemical structure.

4.3. Nanoroads

So far we have assumed that graphene nanoribbons are formed by cutting a piece of graphene into a narrow strip. Another way to define a nanoribbon was proposed in Ref. [99]: to sculpture a graphene nanoribbon by removing hydrogen atoms

Table 5

Gap values for the armchair nanoribbons of different widths found using the density functional theory, from Ref. [80]. The quantity $\sqrt{3}a_0$ represents the lattice constant. The gap of the armchair nanoribbon oscillates with its width; however, the gap is never zero. The details of the oscillations depend on the edge functionalization (for example, in Ref. [80], both pristine and monohydrogenated armchair nanoribbons are discussed). The largest values of the gap are quite insensitive to functionalization. In order to have a gap value similar to known bulk semiconductors, a very narrow armchair nanoribbon must be used. These results were reconsidered in Ref. [84], where it was claimed that density functional theory underestimates the gap, and that the use of the so-called GW approximation [98] is more appropriate. Within the GW framework, the values of the gap substantially increase.

Armchair nanoribbon energy gap			
Energy gap (eV)	Bulk semiconductors with similar values of the gap	Width (nm)	Width [$\sqrt{3}a_0$]
0.7	Ge, InN	2–3	8–12
From 1.1 to 1.4	Si, InP, GaAs	1–2	4–8

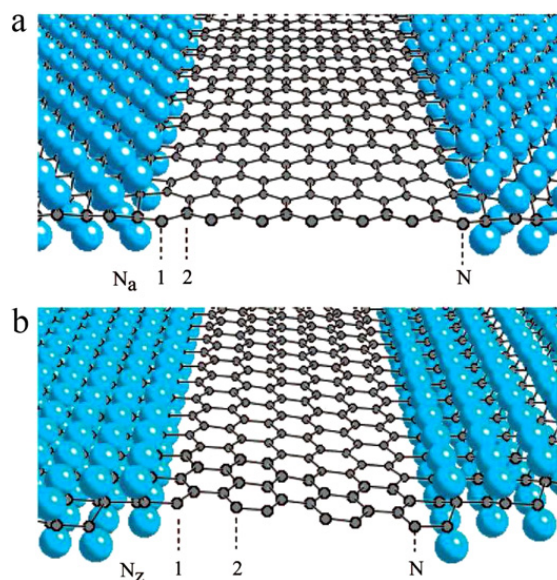


Fig. 11. (Color online) Nanoroads (i.e., graphene nanoribbons bounded by two graphene/graphane interfaces), from Ref. [99]. Small dark balls are carbon atoms, while the large blue balls are hydrogen atoms. The armchair nanoroad is on panel (a), while the zigzag nanoroad is on panel (b). The quantities $N_a = 1, \dots, N$ and $N_z = 1, \dots, N$ characterize the width of the nanoroads. For the nanoroad on panel (a) $N = 13$, while $N = 6$ for the nanoroad on panel (b).

Source: Reprinted with permission from: K. Singh and B.I. Yakobson, *Nano Lett.* **9**, 1540 (2009).
© 2009, American Chemical Society.

along a narrow strip inside a wider graphane sample, as shown in Fig. 11. In such a case, a nanoribbon, called nanoroad in Ref. [99], is bound by two graphene/graphane interfaces, which are discussed in Section 3.3.

As it was established in Ref. [66], the graphene/graphane interface remains almost atomically sharp even at high temperatures. This makes nanoroads a promising candidate to observe ballistic transport.

The magnetic and electronic properties of graphene nanoroads, including the effects of spin–orbit coupling, were discussed in Refs. [99–102]. In Ref. [99] the electronic structure of nanoroads was studied using DFT. It was found that the armchair-type nanoroads are semiconducting. As for zigzag nanoribbons, when they are wide enough they demonstrate edge magnetism. Zigzag nanoribbons are semiconducting in the antiferromagnetic state and metallic in the ferromagnetic state.

Several other works also used DFT to analyze nanoroad properties. In Ref. [100], the zigzag nanoroad stability and electronic structure were investigated, and it was established that even extremely narrow zigzag nanoroads are stable. Narrow nanoroads are always semiconducting due to Peierls instability, which opens a gap. A similar mechanism is responsible for the gap in polyacetylene. Ref. [101] studied the adsorption of hydrogen on a graphene nanoribbon, also formulating the rules governing such adsorption. It was proposed to use such process in order to create narrow nanoroads.

Ref. [102] showed that, due to enhanced spin–orbit coupling at the interface, a nanoroad might be used to convert spin polarization into valley polarization and vice versa. Such a device can operate at temperatures of about 1 K.

The theoretical research summarized in this subsection indicates that nanoroads may be an attractive alternative to usual nanoribbons, able to sustain ballistic propagation of electrons, and also exhibit unusual spin features.

4.4. Transport properties of nanoribbons

For applications, such as FET [77,78], the transport properties of graphene nanoribbons must be investigated. A study of the conductance through a pristine nanoribbon within the framework of the Landauer formalism was presented in

Ref. [103] (see also the review [104]). In such a case, the nanoribbon's conductance is quantized: it changes in discrete steps when the gate voltage is varied. For zigzag nanoribbons it was found that, when the gate potential is tuned to the charge neutrality point (i.e., the Fermi energy is at the apex of the Dirac cone), the conductance is finite due to the edge states. These are the only current-carrying modes under such conditions. Ref. [103] studied the transport through metallic (zero-gap) armchair nanoribbons. Since it is understood now that, strictly speaking, all armchair nanoribbons are semiconducting (see Section 4.2), the results obtained for such objects are valid as long as the gap may be neglected, e.g., when the temperature exceeds the gap. Another study of electron transport through a disorder-free short-and-wide nanoribbon was presented in Ref. [105]. Its findings compared well with the experiments in Ref. [106]. It was concluded in Ref. [106] that the electron propagation in graphene is ballistic up to lengths of the order of 1 μm .

However, in a typical experimental situation ballistic propagation can be spoiled both by edge disorder [107–110] and bulk disorder [107,110]. For bulk disorder, it was found that electron transport is rather insensitive to long-range disorder. Yet, when the disorder becomes short-range, it leads to Anderson localization and to destruction of the ballistic propagation [107,110].

If a nanoribbon is sufficiently narrow, the edge disorder is important [107–110]. The armchair nanoribbons are more sensitive to edge disorder than the zigzag nanoribbons [107,110]. Ref. [108] reported that when edge disorder is present, the difference between transport properties of the armchair and zigzag nanoribbons disappears. These results suggest that to experimentally produce a ballistic nanoribbon one has to overcome very stringent limitations on the edge purity [110]. However, for a semiconducting armchair nanoribbon of finite length one can optimize the width so that the localization effects are, to some extent, masked [109].

Doping [111] and edge functionalization [88,112] affect the transport as well. For example, if a finite-length armchair nanoribbon has a gap induced by the edge-bond deformations (see Section 4.2), then a suitably chosen chemical disorder at the edges may actually increase the conductivity by effectively closing the gap [88]. Namely, if the edges are functionalized with two different kinds of radicals randomly distributed along the length of the ribbon, then the term of the Hamiltonian responsible for the opening of the gap becomes disordered, and the gap closes when this term vanishes on average. Clearly, one has to counteract the Anderson localization in such a situation. Fortunately, this phenomenon is not important for a nanoribbon of sufficiently short length. Transport through this nanoribbon is effectively metallic [88].

Ref. [86] pointed out that for nanoribbons with very corrugated edges the interaction effects can seriously affect the charge transport. According to Ref. [86], a nanoribbon with corrugated edges can be viewed as a series of weakly coupled quantum dots defined by the random geometry of the edges. Electron transport through such system is limited by the Coulomb blockade effect in these dots.

Recent experiments [113–116] on gated nanoribbons discovered that there is a Fermi energy interval where the conductance is suppressed, see Fig. 12. This phenomenon is called the transport gap. It was pointed out in Ref. [114] that the size of the experimentally observed transport gap is too big to be consistent with conclusions of simple one-particle nanoribbon models, where the gap is generated due to the transverse quantization. To develop a more realistic description, the effect of both disorder and interactions must be accounted for, in addition to the transverse quantization. It was proposed that the transport occurs through tunneling between consecutive “charge puddles”, which are the areas with non-zero charge induced by the external disorder potential.

Our discussion shows that transport properties of the nanoribbons are affected most prominently by bulk and edge disorder, transverse quantization, edge type, and interactions.

5. Quantum dots

Quantum dots formed in semiconductor heterostructures have been studied extensively because they are considered promising candidates for applications in optoelectronics on the nanometer scale [117–121]. For instance, dots might be used in detectors, diodes, memory and laser devices. Furthermore, single-electron transport devices which make use of quantum dots could be employed as transistors, and spin-based dot devices might be useful for quantum logic gates. Electrons confined in usual semiconductor dots, with a typical size of a few hundreds of nanometers, are described by the Schrödinger equation and most of their electronic properties are now well-understood and have been experimentally studied by many research groups.

The physics of graphene quantum dots is very different from that in usual semiconductor dots. The reason is twofold: (i) charge carriers in graphene are massless and obey the relativistic 2D Weyl–Dirac equation (3), and (ii) the different configurations of the carbon atoms at the boundaries of the dot affect significantly the dot properties. There are two basic methods of defining a graphene quantum dot. In the first method, the dots are defined by the actual geometry of the graphene layer and they are usually referred to as graphene islands. In the second method, the dots are defined through the application of electric and magnetic fields. Of course quantum dots can also be defined by combining these two methods and recently some other ideas have been put forward for dot formation, which for example include the application of strain to the graphene sheet, a spectral gap opening, and even chemical techniques.

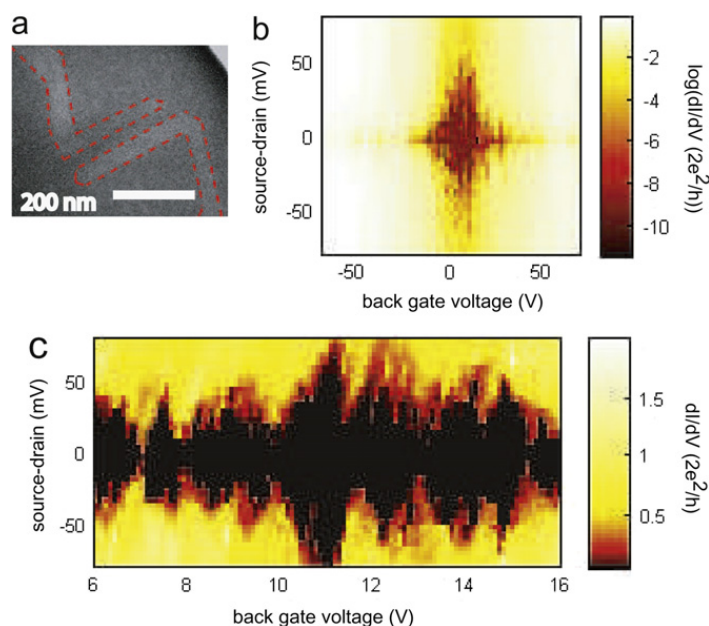


Fig. 12. Graphene nanoribbon (a) and the nanoribbon's electrical conductance data (b, c), from Ref. [115]. Panel (a) shows a nanoribbon defined by etching a graphene sheet. The darker area is graphene, while the lighter areas inside the red dashed lines are graphene-free. In panel (b) the differential conductivity is plotted as a function of the back-gate voltage and source-drain voltage. Note that for small source-drain voltage the conductivity remains suppressed (dark area) for small back-gate voltages, and grows when the latter exceeds a certain value. This is a manifestation of the transport gap. In panel (c) the same data is plotted in a smaller back-gate voltage window. The plot has the characteristic shape of overlapping noisy “Coulomb diamonds”, suggesting that the transport occurs through several “charge puddles” acting as quantum dots.

Source: Reprinted with permission from: K. Todd, H.T. Chou, S. Amasha, and D. Goldhaber-Gordon, *Nano Lett.* **9**, 416 (2009). © 2009, American Chemical Society.

5.1. Geometry-induced dots and graphene islands

It is now possible to mechanically cut (i.e., etch) a graphene flake into various shapes of a few tens of nanometers, which can confine electrons and thus act as quantum dots. These geometry-induced dots or graphene islands have well-defined discrete energy levels whose spectrum depends on the size, shape and the edge type of the dot. Further, disorder and interaction effects are also important for the electronic properties of any realistic graphene system.

A range of typical dot geometries including triangular, hexagonal, rectangular and circular have been studied numerically, mainly within the tight-binding and DFT models [122–129]. In some cases exact analytical solutions are also possible [130–132]. For example, for a triangular armchair dot, exact tight-binding eigenfunctions and eigenenergies were obtained, and a technique for matrix element calculation was developed [132] (see Fig. 13). Quantum dots with arbitrary shapes have also been examined [133].

An important feature of the nano-islands is the appearance of degenerate zero-energy states that are mostly localized at the edges, as predicted for triangular and circular zigzag dots, as well as rectangular dots [122–126,129]. For triangular dots there is a sublattice imbalance, i.e., $N_Z = N_A - N_B \neq 0$, where $N_A(N_B)$ is the number of carbon atoms of sublattice $\mathcal{A}(\mathcal{B})$, and this condition is sufficient in order to have N_Z zero-energy states [124]. The number of these states is proportional to the size of the edges which, in principle, can be made quite large.

Nanostructures with degenerate zero-energy states are useful for applications, since the electrons inside such structures may order magnetically. Magnetism is a consequence of the Coulomb interaction and Hund's rule. For example, the ground state of rectangular dots can support antiferromagnetic ordering whereby the magnetic moments are localized at the zigzag edges with opposite orientation (for edge magnetism, see also the previous section). As shown in Ref. [125] for rectangular dots there is a critical minimum width between the zigzag edges that gives rise to magnetic ordering. If the width is smaller, then the state is nonmagnetic. On the other hand, triangular zigzag dots favor ferromagnetic ordering (see Table 6).

Interestingly, external uniaxial strain on square dots enhances the magnetization and leads to a spatial displacement (drift) of the magnetization from the zigzag to the armchair edges [123]. A magnetization enhancement of 100% was predicted for a strain on the order of 20%, which might be possible to induce by mechanical methods [134].

Moreover, it was theoretically predicted that the edge-state magnetism is robust to impurities and edge-defects, and survives even to irregular structures as long as there are three to four repeat units of zigzag edges [126]. A similar conclusion was reached in Ref. [61]. Some examples of magnetic structures for different dots are presented in Fig. 14. The results are derived from the mean field analysis of the Hubbard model [126].

Another promising property, which may be used in memory devices, is that the spin relaxation time can be long enough, as shown for triangular dots. In general, the spin relaxation time increases with the interaction strength and system size, but remains long even for a relatively small system [122].

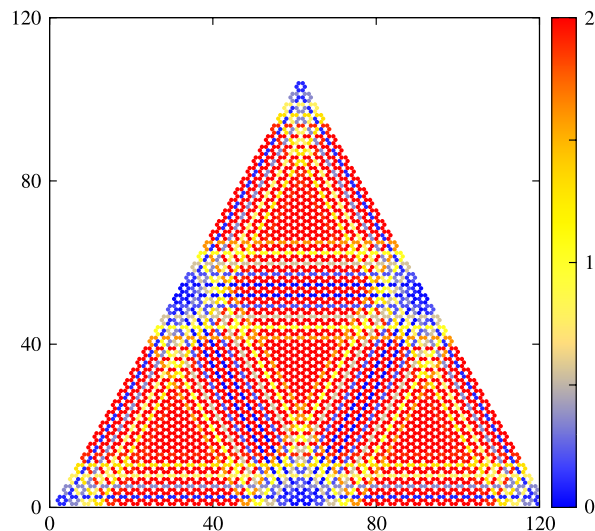


Fig. 13. The Schrödinger equation for the tight-binding Hamiltonian on a triangular armchair quantum dot can be solved exactly [132]. Moreover, the algebraic structure of the wave functions found is sufficiently simple to allow for analytical expressions for some matrix elements. In this figure the exact probability density for certain electron eigenstate on a triangular quantum dot is plotted.

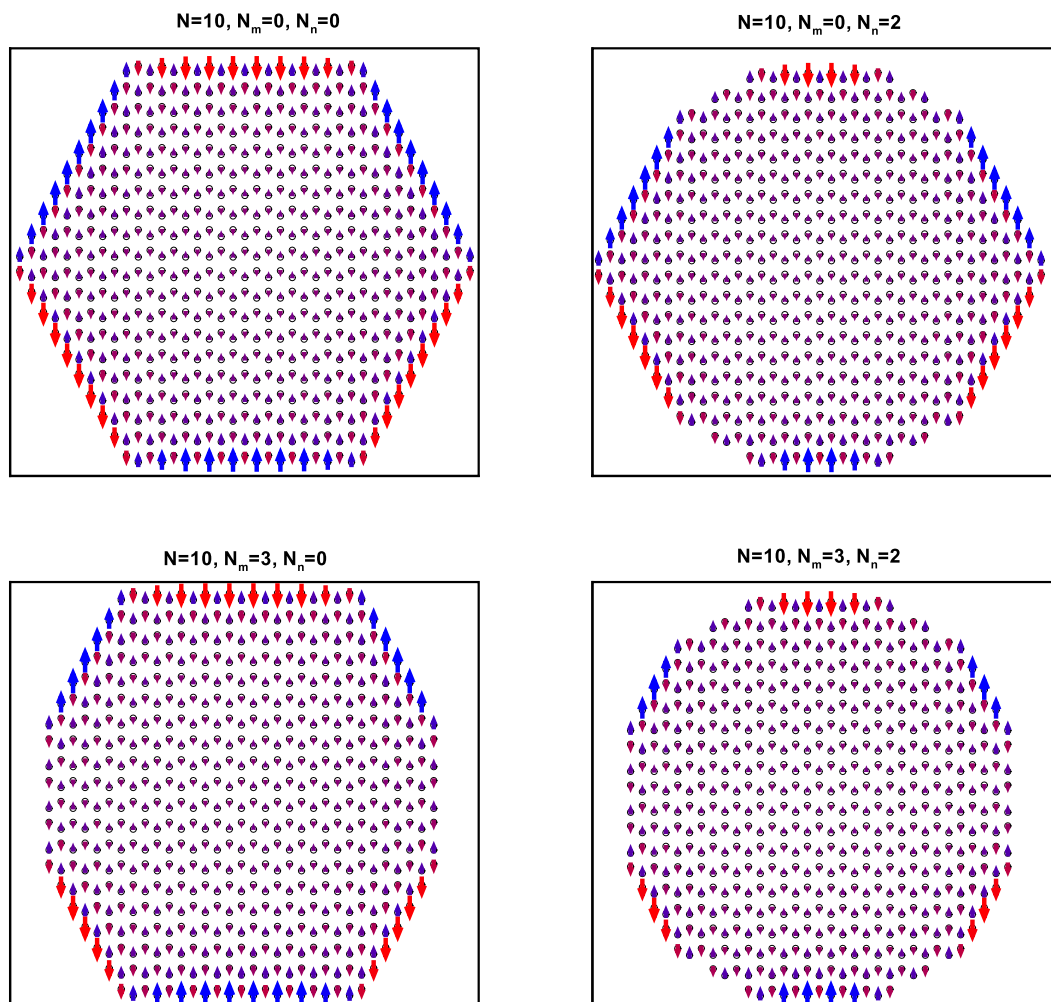


Fig. 14. (Color online) Magnetic properties of graphene dots were investigated numerically in Ref. [126] within the framework of a mean field theory of the Hubbard model. Expectation value of the spin magnetization S^z in four different dots. The size of the arrows is proportional to the magnitude of the magnetic moment. In this figure, N , N_m and N_n denote the size of the dot in the perfect hexagon configuration, the number of armchair edges per vertical side, and the number of armchair edges per slanted edge, respectively. The magnetic moments are much larger at the zigzag edges than at the armchair edges and the internal sites.

Source: Reprinted with permission from S. Bhowmick and V.B. Shenoy, J. Chem. Phys. **128**, 244717 (2008).
 © 2008, American Institute of Physics.

Table 6

Graphene dots have attracted considerable theoretical interest. Various geometries were examined and degenerate zero-energy edge states were predicted for triangular zigzag and rectangular dots (the rectangular dot is defined by two zigzag and two armchair edges). These states are mainly localized at the zigzag edges having only a small amplitude at the center of the dot. Edge states are absent at armchair edges. The existence of such states leads to magnetic ordering that critically depends on the specific geometry. For rectangular dots there exists a minimum width between the two zigzag edges for stable antiferromagnetic ordering [125]. The magnetic properties of the geometry-induced dots are robust to defects and impurities of the edges, can survive to irregular structures [126], and can be tuned by the application of an external strain [123].

Graphene dots or islands (theoretical studies)		
Type	Zero-energy edge states	Magnetic ordering
Triangular	Yes	Ferromagnetic
Hexagonal	No	No
Parallelogram	No	No
Rectangular	Yes	Antiferromagnetic

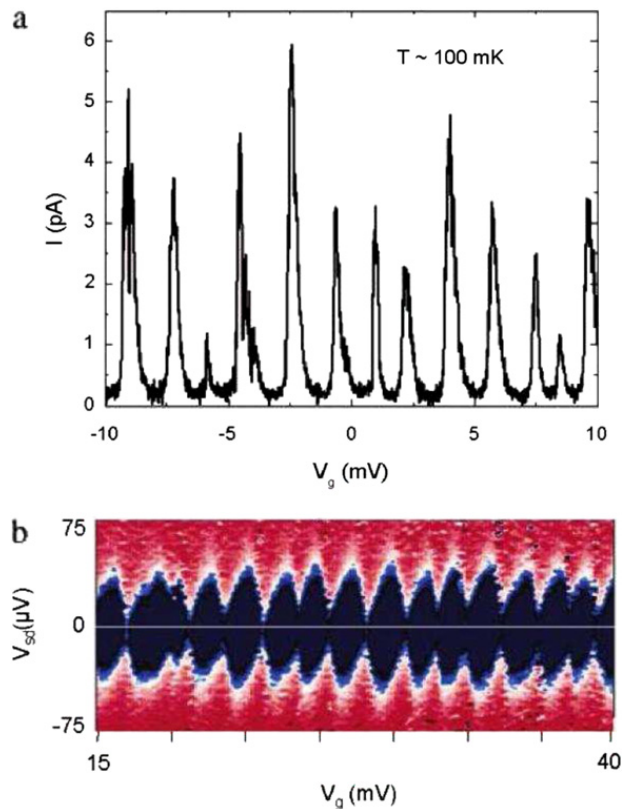


Fig. 15. (Color online) Gated graphite quantum dots were fabricated and low-temperature electrical transport measurements were performed [135]. (a) Current versus gate voltage V_g with source-drain bias $V_{sd} = 10 \mu\text{V}$ at temperature $T \sim 100$ mK. Coulomb oscillations are observed with a period in gate voltage of $\Delta V_g = 1.5$ mV. (b) The differential conductance (dI/dV_{sd}) is plotted as a color scale versus gate voltage (V_g) and source-drain bias V_{sd} . Blue (red) signifies low (high) conductance. The charging energy of the dot is equal to the maximum height of the diamonds: $\Delta V_{sd} = 0.06$ mV.

Source: Reprinted with permission from J.S. Bunch, Y. Yaish, M. Brink, K. Bolotin, and P.L. McEuen, *Nano Lett.* **5**, 287 (2005).
© 2005, American Chemical Society.

Ref. [135] reported low-temperature electrical transport measurements on gated quasi-2D graphite quantum dots. These were the first measurements on mesoscopic samples of graphite which consists of many stacked layers of graphene held together by weak van der Waals forces. Coulomb charging phenomena were demonstrated with the help of data in Fig. 15, where the electrical current through the dot as a function of gate voltage and source-drain bias is plotted. More recent experiments probed the energy spectrum of quantum dots formed in a single layer of graphene [136–138]. An all-graphene single-electron transistor, exhibiting Coulomb-blockade behavior, was operational well-above liquid-helium temperatures [136]. The Coulomb-blockade peaks are (nearly) periodic as a function of gate voltage for large islands (> 100 nm), and nonperiodic for small ones (< 100 nm). The distance between the peaks is proportional to the sum of charging and confinement energies. The former, being typically constant for a specific dot geometry, dominates for large islands [136]. For small islands the size quantization becomes important, and the confinement energy prevails, leading to nonperiodic peaks (see Table 7). The energy-level statistics of graphene islands was also probed, and it was shown to agree well with the theory of chaotic Dirac billiards [136].

Coulomb-blockade measurements on a graphene island (~ 200 nm) with an integrated charge detector were also reported [139] (see Fig. 16). A nanoribbon placed 60 nm from the island acts as a detector, which enhanced the resolution of

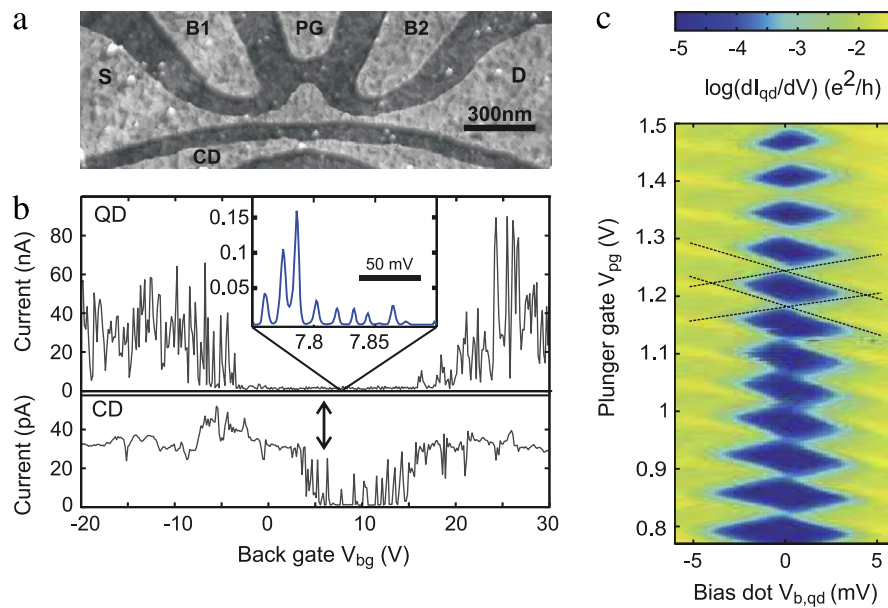


Fig. 16. (Color online) Graphene quantum dot device with charge detector and transport measurement data [139]. (a) Scanning force micrograph of the measured device. The central island, that acts as the quantum dot (QD), is connected to source (S) and drain (D) contacts via two narrow constrictions. The diameter of the dot is 200 nm and the constrictions are 35 nm wide. The charge detector (CD) is a graphene nanoribbon and the lateral gates B1, B2 and PG are used to tune the device. (b) Current as a function of back-gate voltage of the QD (upper panel) and CD (lower panel). The source-drain voltage is 500 μ V and the temperature is 1.7 K. The inset shows typical Coulomb-blockade features as expected in a dot device. (c) Differential conductance is plotted as a color scale versus source-drain bias and PG gate voltage, for a back-gate voltage of 2 V. The charging energy was estimated to be about 4.3 meV. *Source:* Reprinted with permission from J. Guttinger, C. Stampfer, S. Hellmuller, F. Molitor, T. Ihn, and K. Ensslin, *Appl. Phys. Lett.* **93**, 212102 (2008). © 2008, American Institute of Physics.

Table 7

Graphene islands were investigated experimentally via electrical transport measurements, and single-electron transport was demonstrated [136]. When the diameter of the island is large ($D > 100$ nm) the Coulomb peaks in the conductance, as a function of back-gate voltage, are periodic and their position is determined mainly by the characteristic charging energy. For small-diameter islands ($D < 100$ nm), the position of the peaks is nonperiodic and the dominant energy scale is the confinement energy on the order of $E_D \sim v_F h / 2D$ (h is Planck's constant). This is much larger than the corresponding energy $E_S \sim h^2 / 8mD^2$ of Schrödinger electrons with effective mass m ; $E_D / E_S \sim 40$ for $D = 100$ nm, and m is the effective mass for GaAs. Stable, robust and conductive dot islands as small as 15 nm were fabricated, showing the potential of graphene for nanoelectronics.

Graphene dots or islands (experimental studies)		
Size of island (D)	Coulomb peaks	Energy scale
< 100 nm	Nonperiodic	Confinement $\sim v_F h / 2D \approx 41$ meV ($D = 50$ nm)
> 100 nm	Periodic	Charging ≈ 3 meV ($D \approx 250$ nm)

single charging events on the island. In addition, tunable double quantum dots were fabricated whereby the coupling to the leads and the interdot coupling were tuned by graphene in-plane gates [140]. Spin spectroscopy has also been investigated in graphene dots [141].

5.2. Field-induced dots

Charge confinement within the “bulk” graphene sheet is tricky due to the Klein tunneling effect [142]. In case of normal incidence, this allows for perfect transmission of massless relativistic particles through high and wide potential barriers. A key point is that in the barrier region the states of massless Weyl–Dirac particles have an oscillatory character, even at energies lower than the potential height, as happens exactly outside the barrier. This is completely different from Schrödinger particles with non-zero mass, for which the states in the barrier region decay exponentially and therefore perfect transmission is not feasible. Experimentally, the Klein tunneling was demonstrated in graphene through electrical transport measurements in steep potential barriers generated by metallic gates [143].

Because of the Klein tunneling, an electrostatic potential minimum in graphene leads to quasi-bound states, i.e., resonant states (see Table 8 for a classification of the dot states) and therefore it is inadequate to confine electrons [144–146]. Nevertheless, the finite lifetime of the states, characterizing the trapping time of an electron in the dot region, can be relatively long. It depends on the potential profile and eigenenergy. A smooth potential and a large angular momentum enhance the lifetime of the quasi-bound states [144,146], as happens also with eigenenergies close to the maximum of the potential barrier [145]. Fig. 17 shows the effect of the quasi-bound states on the local density of states of a circular dot.

The electrostatic confinement of electrons in graphene dots was also examined through the dependence of the conductance on the dot area, which is tunable with a metal gate [147]. Both disc-shaped dots, in which the classical dynamics

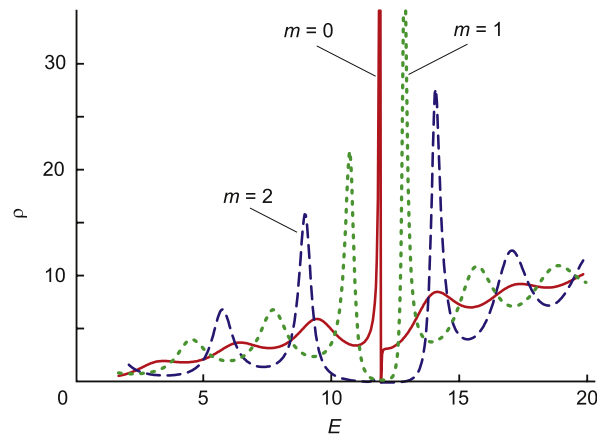


Fig. 17. (Color online) The physics of quasi-bound states in circular graphene dots was examined theoretically by solving the Weyl–Dirac equation [145]. The figure shows the local density of states as a function of energy in the case of a barrier height of $V = 12$ (dimensionless units) for three angular momentum numbers: $m = 0$ (solid curve), $m = 1$ (dotted curve), and $m = 2$ (dashed curve). The peaks become narrower as the momentum increases, within a specific energy range, thus the lifetime of the corresponding states becomes longer. Notice the very narrow peak when the energy is close to the barrier height (for $m = 0$), as a consequence of the total reflection of the wavefunction at the dot edge.

Source: Reprinted figure with permission from A. Matulis and F.M. Peeters, Phys. Rev. B **77**, 115423 (2008). © 2008, by the American Physical Society.

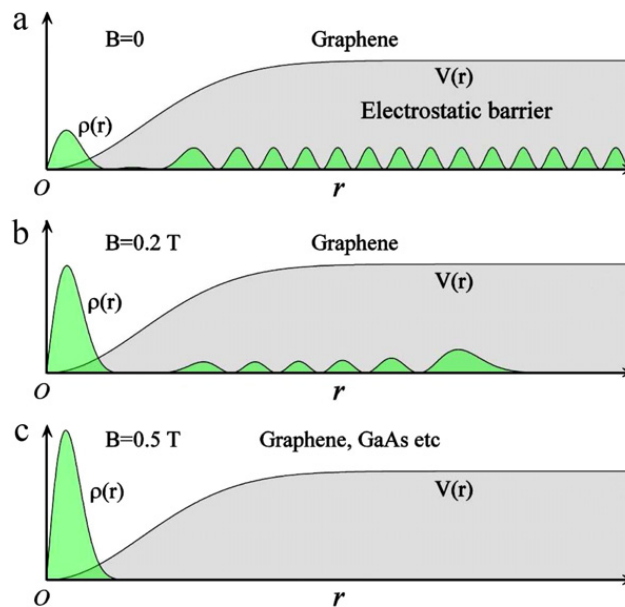


Fig. 18. (Color online) Klein tunneling in a circular graphene quantum dot in a uniform magnetic field. The dot is defined by the electrostatic potential $V(r)$, which vanishes at the center (O) of the dot and asymptotically rises to a constant value, while the magnetic field B is perpendicular to the graphene sheet. (a) For $B = 0$ and small angular momentum, the radial probability distribution $\rho(r)$, for one of the spinor components, has a large amplitude near the center of the dot and oscillates inside the barrier region because of the Klein tunneling. In this case, which is unique to graphene, the quantum state is quasi-bound and has an oscillatory asymptotic character. (b) When the magnetic field is non-zero, the Klein tunneling is partially suppressed. At large r the oscillatory behavior is replaced by exponential decay, indicating that the state is bound. As in (a), this case is also unique to graphene. (c) With increasing magnetic field, the Klein tunneling is completely suppressed and the probability distribution decays exponentially inside the electrostatic barrier. The state is now bound near the center of the dot and such a state can be seen in both graphene dots and usual semiconductor dots, e.g., GaAs. For the latter, this state can be seen even when $B = 0$. A magnetic-field-induced confinement-deconfinement transition in a graphene dot due to the Klein tunneling was theoretically examined in Ref. [148].

is regular, and stadium-shaped dots where the classical dynamics is chaotic were studied. Confinement can be achieved only in the former when the corresponding Weyl–Dirac equation is separable.

The application of a magnetic field can completely suppress the Klein tunneling, leading to bound states [148,150–152]. Thus graphene quantum dots can be formed with the help of a nonuniform magnetic field, whereby the field is zero within a disc area defining the spatial region of the dot, and nonzero outside the dot [150]. The combination of an electrostatic potential and a vector magnetic potential allows the confined-deconfined character of the dot states to be tuned at will [148]. Most interestingly, it allows graphene dots to be formed in a uniform magnetic field using standard gate electrodes as in common semiconductors [148]. Then the quantum states can be tuned with the strength of the magnetic field and this property allows the Klein tunneling mechanism to be probed experimentally in graphene dots. A dot design suitable for this

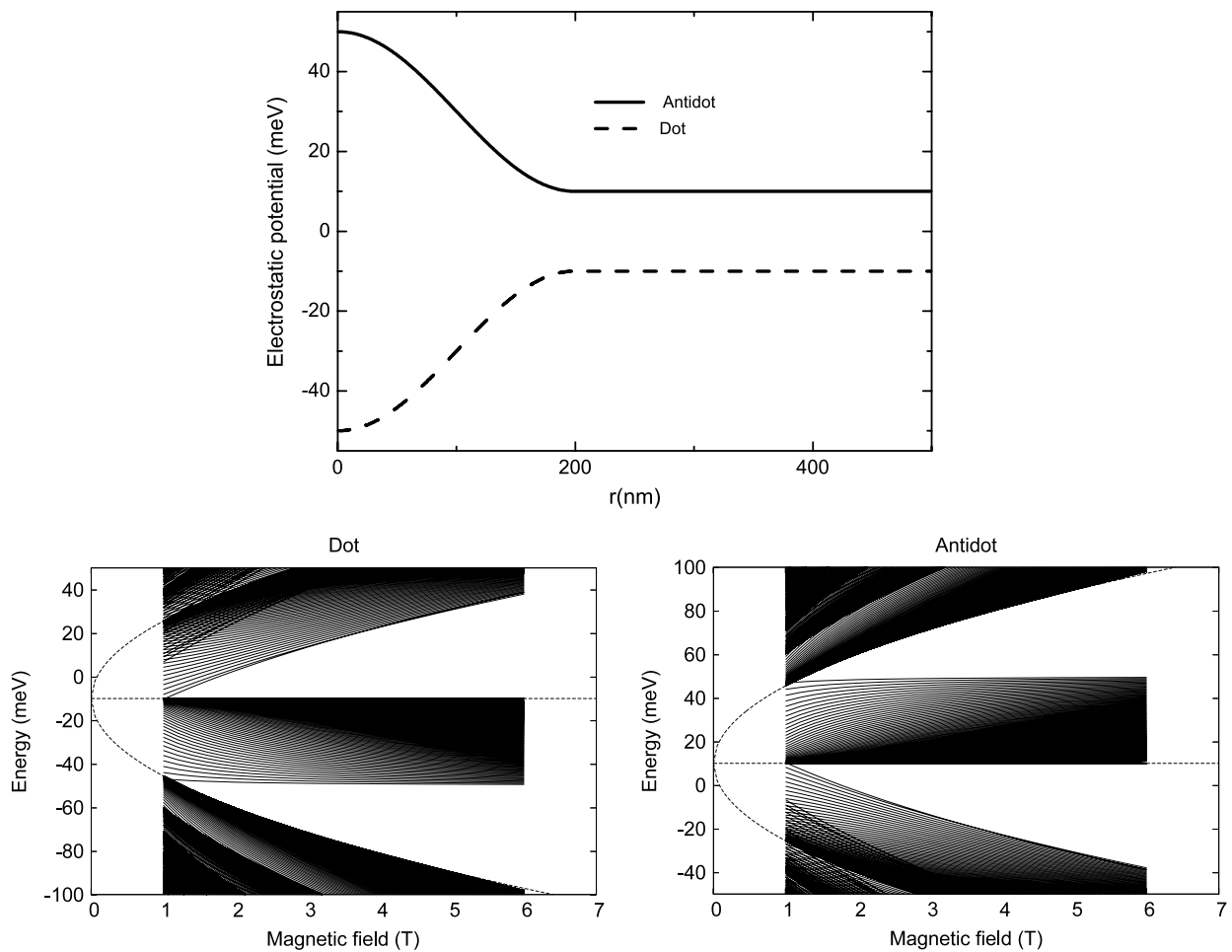


Fig. 19. A graphene dot or an antidot can be formed with the help of a uniform magnetic field applied perpendicular to the graphene sheet [149]. (top) The electrostatic potential profile of an antidot (solid line) and a dot (dashed line) along the radial direction. Energy spectra as a function of the applied magnetic field of dot (left) and antidot (right). The dashed lines show the Landau levels of an ideal graphene sheet. The potential is adjusted so that the confined dot (antidot) states lie in the gap between Landau level 0 and Landau level -1 ($+1$). The symmetry between the energy levels ($E \rightarrow -E$) of the two systems is a direct consequence of the Dirac cone band-structure in graphene.

Source: Figure is reprinted from: P.A. Maksym, M. Roy, M.F. Craciun, S. Russo, M. Yamamoto, S. Tarucha, and H. Aoki, *J. Phys.: Conf. Ser.* **245**, 012030 (2010).

experiment was suggested in Ref. [148]. Fig. 18 illustrates the magnetic field-induced suppression of the Klein tunneling for an electron inside a dot, and Table 9 summarizes the general conditions for confinement in a circular quantum dot, as derived in Ref. [148]. The physics of electrostatic barriers in the presence of uniform and nonuniform magnetic fields is analyzed in Section 7.

The concept of defining a magnetic graphene dot was further developed theoretically in Ref. [149]. In particular, in a strong magnetic field the electrostatic potential of the dot is adjusted so that the confined dot states lie in the gap between Landau level 0 and Landau level -1 (see Fig. 19). This ensures that the dot states are energetically isolated in a region of low density of states and thus they can be probed using standard charge-sensing measurements as in a GaAs dot. Numerical estimates showed that a typical spacing between the dot levels is ~ 2 meV at a magnetic field of 5 T. In addition, Ref. [149] considered how this basic idea can be extended to a graphene antidot for which the levels of the confined states lie in the region between Landau level 0 and Landau level $+1$. For a confined state with energy E in the dot, there is a corresponding confined state with energy $-E$ in the antidot. This is a unique property of graphene due to the symmetry of the Dirac cone. The physics of graphene antidots in a magnetic field was also examined in Ref. [153].

5.3. Nanoribbons of graphene and dots

As discussed in the previous section, the most commonly studied graphene nanoribbons are either of armchair or zigzag type. A quantum dot defined by an external electrostatic (parabolic) potential along the nanoribbon was investigated theoretically in Ref. [154]. Quasi-bound states inside nanoribbons with either zigzag or armchair edges, in both metallic and semiconducting samples, were predicted. The lifetime of such states can be made long enough by increasing the characteristic length of the external potential, for example, with a gate electrode. Further, the dependence of the conductance on the gate voltage was found to be sensitive to the type of edges as illustrated in Fig. 20. The proposed device can operate

Table 8

The quantum states of a dot, formed within the “bulk” graphene sheet, can be either bound or quasi-bound. Because of the Klein tunneling, both types of states can have a large amplitude in the barrier region of the quantum dot, though their asymptotic behavior is different. Exponential decay is characteristic of bound states, whereas oscillatory behavior is characteristic of quasi-bound states. As shown in Ref. [148] the type of states can be tuned with an electrostatic potential and a uniform magnetic field perpendicular to the graphene sheet (see also Table 9).

Quantum dot states		
Type (other used names)	Lifetime	Spatial asymptotic behavior of wavefunction
Bound (confined, stable)	Infinite	Exponential decay
Quasi-bound (deconfined, resonant)	Finite	Oscillatory

Table 9

Confinement of electrons in a circular graphene dot is conditional because of the Klein tunneling [148]. Consider a graphene dot defined by the electrostatic potential $V = V_0 r^s$ and the magnetic vector potential $\mathbf{A} = (0, A_\theta, 0)$, with $A_\theta = A_0 r^t$ and $s, t > 0$. In such a situation, if asymptotically $A_\theta < V$, then the quantum states are quasi-bound; if $A_\theta > V$, they are bound. In the special case $A_\theta \sim V$, the states are bound only when $V_0 < v_F e A_0$ (e is the absolute value of the electron charge). This suggests that the states can be tuned at will with an electric or magnetic field. A simple limit occurs for a constant potential ($V = \text{const.}$) and uniform magnetic field B perpendicular to the graphene sheet ($t = 1, A_0 = \frac{B}{2}$). Then the states are always bound and correspond to the well-known Landau levels.

Circular graphene dot: $V = V_0 r^s, A_\theta = A_0 r^t$		
Asymptotically	s, t	Dot states
$A_\theta < V$	$t < s$	Quasi-bound for all V_0, A_0
$A_\theta \sim V$	$t = s$	Quasi-bound for $V_0 > v_F e A_0$
$A_\theta \sim V$	$t = s$	Bound for $V_0 < v_F e A_0$
$A_\theta > V$	$t > s$	Bound for all V_0, A_0

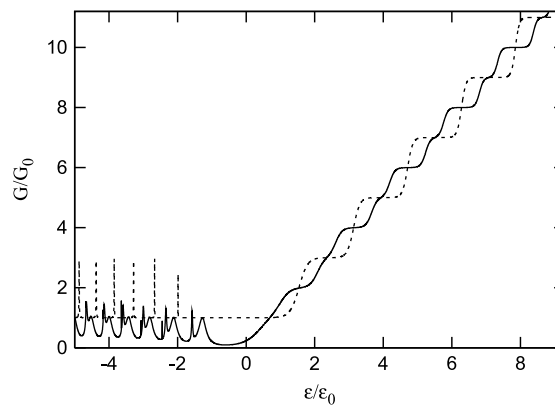


Fig. 20. Theoretical studies showed that a graphene quantum dot can be formed by an external electrostatic potential in a nanoribbon system [154]. The conductance through the dot as a function of the Fermi energy depends on whether the system is semiconducting (solid line) or metallic (dashed line). In both cases, the nanoribbons have armchair edges. For $\varepsilon < 0$ the device operates as a quantum dot and the conductance exhibits resonances. For $\varepsilon > 0$ the device operates as a point contact and the conductance exhibits steps. For $\varepsilon > 0$ the conductance steps in the semiconducting system are twice smaller than those in the metallic.

Source: Reprinted figure with permission from P.G. Silvestrov and K.B. Efetov, Phys. Rev. Lett. **98**, 016802 (2007). © 2007, by the American Physical Society.

either as a quantum dot or as a point contact. For the former, the conductance displays resonances at negative Fermi energy, whereas for the latter it has a step-like behavior at positive Fermi energy. The conductance steps in the semiconducting system are twice smaller than those in the metallic system.

Semiconducting nanoribbons with armchair edges were proposed for the formation of spin qubits in graphene dots [155,156]. Confinement in one direction is achieved naturally by the nanoribbon and in the second direction electrically by gate voltages. In this set-up, the valley degeneracy is lifted, thus allowing Heisenberg spin exchange coupling in tunnel-coupled dots. Such graphene dots can be coupled over long distances as a consequence of the relativistic nature of electrons in graphene, exhibiting Klein tunneling.

The electrostatic confinement of electrons in graphene nanoribbons as well as the Coulomb-blockade effect were experimentally demonstrated [157]. In particular, electrons are confined between gate-induced pn -junctions acting as barriers. However, even when no pn -junctions are formed, the electrons are still confined, though in a larger area due to strong disorder.

5.4. More dots

Tunable quantum dots which take advantage of a gap in the energy dispersion were also proposed in both monolayer and bilayer graphene [158–161]. Experimentally, the gap can be introduced via a chemical and/or electrical technique [25,26]

(see also Table 2), and it allows dots to be formed electrostatically in a quite similar manner as in common semiconductors. A finite gap introduces a mass term in the Weyl–Dirac Hamiltonian. Then for a dot-confining potential with a finite asymptotic value, the gap gives rise to an energy range within which the Klein tunneling is suppressed, leading to the formation of bound states. In this energy range, which is directly proportional to the value of the gap, hole states do not exist and therefore the electron states decay exponentially. Moreover, for quantum dots formed in the gapped sample the valley degeneracy is lifted by a uniform magnetic field. This property might be attractive in order to define spin and valley qubits [158].

It was also shown theoretically that a spatially modulated Dirac gap in the graphene sheet can lead to confined states with discrete energy levels, thus giving rise to a dot. The basic advantage of this proposal is that the dot is formed without applying external electric and/or magnetic fields [160]. Thus magnetic fields can be used to manipulate the spin states without affecting the confinement of the corresponding orbital states. The properties of a Dirac gap-induced graphene dot in the presence of an electrostatic quantum well potential were studied in Ref. [161]. It was shown that confined states which are induced thanks to the spatially modulated Dirac gap couple to the states induced by the potential. The resulting hybridized states are localized in a region which can be tuned with the potential strength; an effect which involves Klein tunneling. Numerical calculations of the local density of states suggest that this effect could be probed [161].

Strain engineering is another proposal in order to generate confinement in a sheet of graphene [162]. Local patterning of the substrate induces in-plane strain in the graphene lattice, anisotropically changing the hopping amplitude between the carbon atoms. As a result, in the continuum approximation the quasi-particles are described by an effective Weyl–Dirac equation in the presence of a gauge field. It turns out that this field can act in a rather similar manner as a magnetic field and therefore it can lead to confined quantum states. A noteworthy advantage of this proposal [162] is that patterning can be made directly on the substrate, hence protecting the graphene layer from possible damage.

Vacancy clusters in the graphene sheet were also suggested for dot formation. In particular, DFT and tight binding calculations showed that cluster of hydrogen vacancies can serve as quantum dots. The stability as well as the shape and size of these dots depend crucially on the graphene/graphane interface energy and the degree of aromaticity [163].

5.5. Quantum rings

Quantum rings in graphene have also attracted some interest, mainly because these types of devices allow the investigation of phase-coherence phenomena, as it is now well-known from studies in usual semiconductor systems.

In a graphene ring device, conductance oscillations versus magnetic field were reported as a consequence of the Aharonov–Bohm effect [164] (Fig. 21). The amplitude of the oscillations increases at high magnetic field in the regime where the cyclotron diameter becomes comparable to the width of the arms of the ring. For temperatures below 1 K the extracted phase-coherence length is comparable to or larger than the diameter of the ring, which is approximately 1 μm .

Theoretical investigations of graphene rings showed that the valley-induced orbital degeneracy is lifted, as a result of the ring confinement and the applied magnetic field [165]. This lifting has observable consequences on the persistent current and the ring conductance. An interesting finding is that the degeneracy can be controlled with the induced Aharonov–Bohm flux, and this can be achieved irrespective of the magnitude (weak or strong) of the intervalley scattering.

Another theoretical work showed that both electrons and holes can be confined in electrostatically formed quantum rings in bilayer graphene [166]. There are two main advantages in this proposal. First, bound states can be created owing to a position-dependent energy gap that suppresses the Klein tunneling. Second, the ring parameters can be tuned by external fields.

The role of Coulomb-induced electron–electron interactions and their interplay with the valley polarization in a graphene quantum ring were also examined [167]. In a few-electron ring, the interactions have a direct signature on the fractional nature of the Aharonov–Bohm oscillations in the persistent current and the absorption spectrum, and therefore they could be observed.

6. Graphene *pn*-junctions and *pnp*-structures

Several graphene-based field-effect devices have been realized in laboratories. Ref. [13] reported the fabrication of a FET made of graphene which operates at a record-breaking frequency of 100 GHz. In Ref. [168] a room-temperature-operated switch demonstrating an on/off ratio exceeding 10^6 was described. Also, the implementation of a digital integrated circuit was reported in Ref. [169]. The microcircuit consists of two transistors and performs the logical inversion operation. A graphene FET used as a biosensor was described in Ref. [170].

All such devices are characterized by a spatially inhomogeneous Fermi level inside the graphene sample. There are several basic types of such systems: interfaces separating regions with different concentrations of the charge carriers (*pp'*-junctions, *nn'*-junctions), or regions with carriers of opposite signs (*pn*-junctions), or series of such interfaces (*pnp*-structure, *pp'p*-structure, etc.). Transport properties of these systems is an important subject of both theoretical and experimental investigations. These studies are reviewed below.

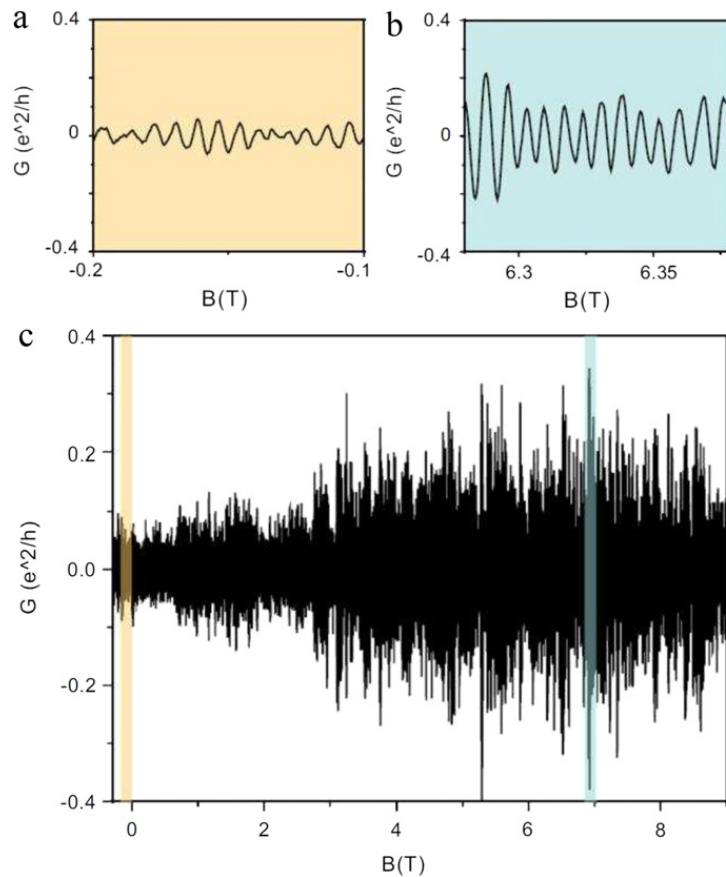


Fig. 21. (Color online) The Aharonov–Bohm (AB) effect was experimentally demonstrated in a graphene ring device [164]. (a)–(c) AB conductance oscillations versus applied magnetic field, for a back-gate voltage of 30 V and temperature of 150 mK. For $B \sim 3$ T, an increase of the AB amplitude is observed. Panel (a) shows a magnified view of the yellow region in (c), while panel (b) expands the blue part in (c).
 Source: Reprinted figure with permission from S. Russo, J.B. Oostinga, D. Wehenkel, H.B. Heersche, S.S. Sobhani, L.M.K. Vandersypen, and A.F. Morpurgo, Phys. Rev. B **77**, 085413 (2008).
 © 2008, by the American Physical Society.

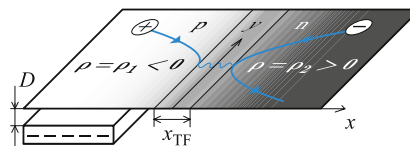


Fig. 22. (Color online) The pn -junction studied in Ref. [173]. There are two gate electrodes in this device. The first one is the semi-infinite gate on the left side. It controls the density drop $\rho_2 - \rho_1$ across the junction. The second electrode is an infinite back gate above the sheet (not shown). It fixes the density ρ_2 at far right. Lines with the arrows show trajectories of an electron (–) and a hole (+). The electron current in n -region is converted into hole current in p -region. Note that the direction of the incident electron current in n -region and the direction of the hole current in p -region are symmetric with respect to y -axis reflection (the same type of refraction is shown in Fig. 23A).
 Source: Reprinted figure with permission from L.M. Zhang and M.M. Fogler, Phys. Rev. Lett. **100**, 116804 (2008).
 © 2008, by the American Physical Society.

6.1. pn -junction

If two planar electrostatic gates separated from the graphene sample by an insulating layer are charged in such a way that the chemical potential at $x > 0$ is shifted above the electroneutrality level and at $x < 0$ below the electroneutrality level, a pn -junction is formed at $x = 0$, see Fig. 22. The simplest model of the electrostatically-defined pn -junction was studied in Refs. [171,172].

In Ref. [171] the current transmission through a pn -junction was investigated. When the current approaches the pn -junction at the right angle, it passes through with no reflection. This is a manifestation of the Klein tunneling. Otherwise, the reflected current appears. The primary source of reflection in such a system is a classically-forbidden strip near the center of the junction, which can be crossed only by quantum tunneling. The strip's width l depends on the incidence angle θ [for normal incidence ($\theta = 0$) = 0, hence, Klein tunneling]. In the model of Ref. [171], parameters of the potential barrier under which the particle has to tunnel depend on the geometry of the pn -junction and the gates' potentials.

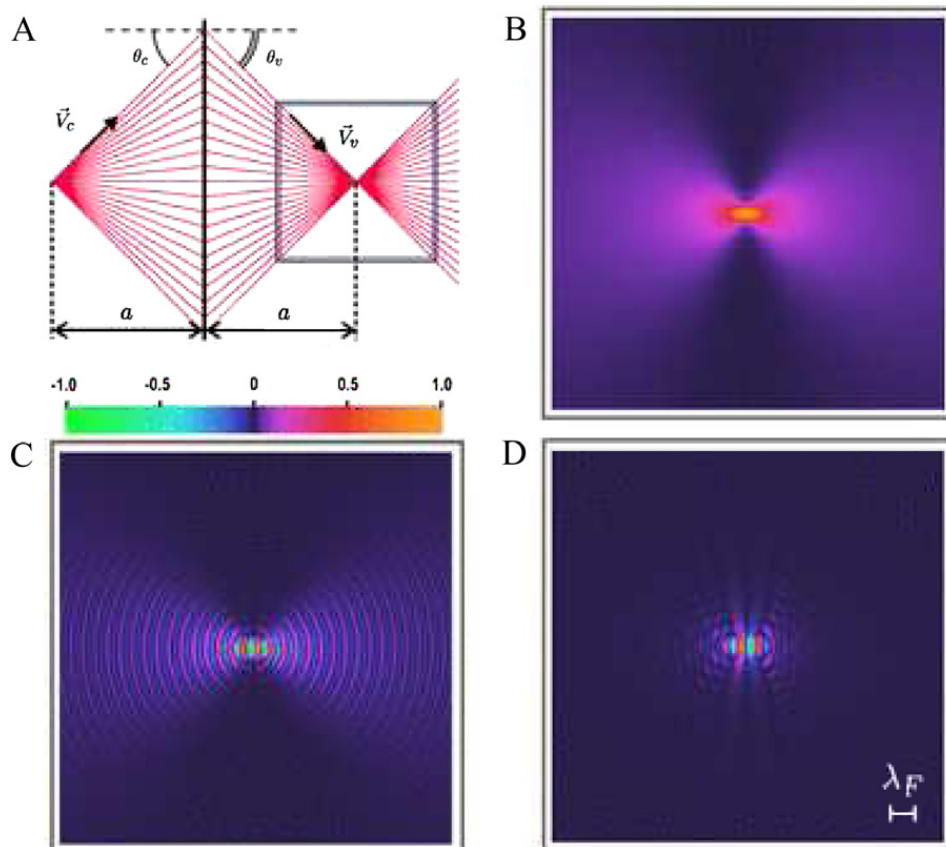


Fig. 23. *pn*-junction as an electron-focusing device, from [179]. If the gates' voltages are such that the concentration of electrons in the *n*-region and the concentration of holes in the *p*-region are the same, a particle hitting the *pn*-junction interface at the incidence angle θ_c would be converted into a hole on the other side of the junction propagating at the refraction angle $\theta_v = -\theta_c$ (see panel A). Under such conditions, a current emanating from a point source is focused into a small spot, "the image" (see panel B), on the other side of the *pn*-junction [179]. When the electron's density is not equal to the hole's density, the focus becomes blurred, and the focal point is shifted along the *x*-axis. This might provide the opportunity to manipulate the location of the focus with the help of the gate voltage. In panels C and D the current distributions affected by different perturbations are plotted [179].

Source: From V. V. Cheianov, V. Falko, and B. L. Altshuler, *Science* **315**, 1252 (2007). Reprinted with permission from AAAS.

The main finding of Ref. [171] was that the current transmission through such *pn*-junction is very sensitive to the angle θ : for normal incidence the transmission is perfect, but it exponentially quickly deteriorates when θ grows. This allows one to create very collimated beams of current. Additionally, the selectivity to θ can be used to detect the magnetic field: since the magnetic field bends the trajectory of a charged particle, then, in a properly designed device, a particle hits the interface at a magnetic-field-dependent angle. As a result, the transmission becomes sensitive to the field. Different devices utilizing properties of the graphene *pn*-junction were proposed in Ref. [171].

The treatment of Ref. [171] was re-examined in Ref. [173]. It was noted there that the non-linear charge screening affects the *pn*-junction characteristics. When the non-linear screening is accounted, significant deviations from the findings of Ref. [171], which neglects many-body effects, are discovered. The results in Ref. [173] indicate that the interaction significantly reduces the *pn*-junction resistance.

A more general study, including not only the electron–electron interaction, but also the disorder, was presented in Ref. [174]. It was shown that, depending on the junction's parameters, it may be in either of three regimes: (i) ballistic, where the *pn*-junction resistance is dominated by the ballistic contribution, (ii) diffusive, where the resistance is dominated by the diffusive contribution, and (iii) the crossover regime, when both ballistic and diffusive contributions are comparable. In Ref. [174] several experimental *pn*-junctions [175–178] were analyzed trying to find junctions in the ballistic regime. It was concluded that the considered experimental systems satisfy the conditions for ballistic propagation only marginally at best. It was suggested that higher mobility or a larger carrier concentration gradient near the junction is required to create a ballistic *pn*-junction.

The ballistic *pn*-junction has attracted considerable attention due to its unusual electron-refraction properties. In Ref. [179] it was observed that, under certain conditions, the electron beam passing through a graphene *pn*-junction experiences refraction in such a manner that the refraction angle equals to *minus* the angle of incidence, see Fig. 23. If this is the case, then current emanating from a point source on one side of the *pn*-junction is focused into "a point image" on the other side of the junction. This situation is similar to the refraction of light at the interface with a metamaterial whose refraction index is minus unity. The focusing properties of the *pn*-junction with circular geometry were investigated in Ref. [180].

However, this ability to focus the electrical current is easy to spoil. Ref. [179] pointed out that at the level of the geometrical optics the focus is perfect only if the density of holes in the p -electrode is the same as the electron's density in the n -electrode. In Ref. [174] it was shown that disorder destroys the focus as well. Finally, since the transmission of a pn -junction decays quickly as the incidence angle deviates from $\pi/2$, only a small fraction of the initial current is able to pass through the junction to form “the image”.

When a graphene pn -junction is placed in a non-uniform magnetic field, it acquires new interesting features. This type of device is discussed in Section 7.

6.2. Doping graphene by contact with metals

In addition to electrostatic doping, it is possible to change the charge density in graphene by making contact with a metal electrode. In such a case, depending on the electrode's material, the electrons either leave the graphene sample to the electrode or flow into the graphene from the electrode.

Junctions created with the help of this kind of doping were investigated experimentally in Ref. [181]. Materials for the metallic electrodes were chosen in such a way as to dope the graphene with holes. Then, depending on the voltage of the back gate, either pp' - or pn -junctions were formed.

The graphene–metal interface was investigated theoretically in Refs. [182–184]. Charge transfer between the metal electrode and the graphene sample was studied in Refs. [185,186] with the help of DFT. According to Ref. [185] the Fermi energy shift inside the graphene sample is a monotonous function of the metal work-function, as one should expect. However, when the work-function of the metal coincides with that of graphene, the graphene sample is not neutral, as one naively might anticipate, but rather it is predicted that the sample is n -doped. This happens because of the chemical interaction between the metal and graphene.

6.3. pn p-structure

The theory of electronic transport in clean pn p-structures was presented in Ref. [172]. There, they demonstrated that the conductance of ballistic pn p-structure exhibits oscillations (‘Fabry–Pérot’ resonances) as a function of the carrier concentration in the middle (n) area of the pn p-structure. These resonances are due to quasi-bound electron states in the n -region of the pn p-structure.

A more general numerical study, which accounts for interaction and impurities, was performed in Ref. [187]. It reported a crossover from ballistic to diffusive regime when the mean-free-path becomes comparable to the length of the middle region. The disorder wipes out the ‘Fabry–Pérot’ resonances. However, it is conceivable that these survive under a small concentration of impurities, and, thus, could be seen experimentally.

A phenomenon analogous to the ‘Fabry–Pérot’ resonances was discussed in Refs. [188,189], where the transmission through several junctions connected in series was studied. Because of electron wave function interference, the transport through such structure demonstrates a non-monotonous dependence on the current incidence angle and the distance between the junctions.

Electrostatically-defined n pn- and pn p-structures were realized experimentally [190–192]. For example, Fig. 24 shows a scanning electron microscope image of a pn p-structure from Ref. [190]. The experimental observation of ‘Fabry–Pérot’ oscillations in pn p-structures was reported in Refs. [190,191]. In Ref. [192] experimental data were analyzed within the theoretical framework of Ref. [171]. Ref. [192] concluded that, in the fabricated pn p-structure, the individual pn -junctions are ballistic, and that the fabrication of a ballistic graphene pn p-structure is feasible.

In the previous subsection we discussed the peculiar electron refraction at the pn -interface. In Ref. [179] several possible applications of this effect were proposed, among which the most known is the so-called “electron Veselago lens”. The latter device is a ballistic graphene n pn- or pn p-structure in which both junctions are tuned to operate in such a manner that the electronic current emitted from a point current source in the left n -electrode travels through two junctions and would be focused into a point (image of the source) in the right n -electrode. A similar phenomenon was predicted by Veselago [193] in the optics of materials with a negative-refractive index: the electromagnetic rays emitted from a point source are focused upon passing through a slab of such material. This slab is called the Veselago lens. It is an analog of the n pn-structure under discussion.

However, the above analogy is incomplete. The “superresolution”, the most advantageous property of the optical Veselago lens [194,195] (see also Ref. [196–199]), is absent for the graphene device [200]. Also, since the current transmission decays quickly for non-normal incidence, the graphene lens is very opaque. This might make its application problematic.

Our discussion in this section suggests that graphene pn -junctions and pn p-structures, due to their interesting properties, may, in principle, be used for current control and magnetic field sensing applications, provided that a way to attenuate the effects of the disorder is found. If a graphene pn p-structure is placed into a non-homogeneous magnetic field, it may, under certain condition, act as a electron waveguide. The relevant discussion can be found in Section 7.3.

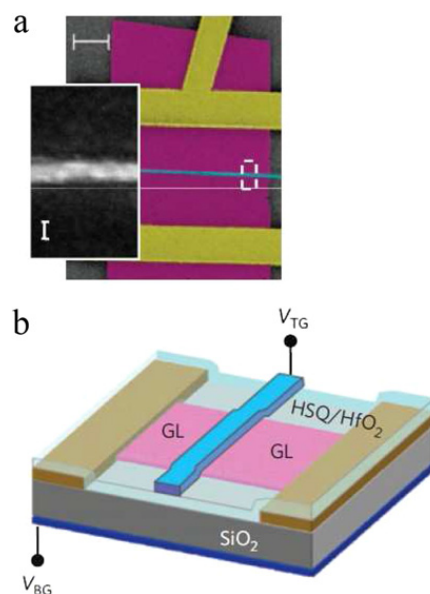


Fig. 24. (Color online) Experimental realization of a graphene *pnp*-structure, from Ref. [190]. Panel (a) shows the scanning electron microscope image of the structure. The large purple rectangle is the graphene sheet. Two bulk yellow electrodes (source and drain) and one narrow blue electrode (top gate) are placed on top of the graphene. The back gate beneath the structure is not visible. The inset presents an enlarged view of the top gate. Panel (b) shows a schematic diagram of the same setup.

Source: Reprinted by permission from A.F. Young and P. Kim, Nat. Phys. 5, 222 (2009).

© 2009, by Macmillan Publishers Ltd: Nature Physics.

7. Quantum barriers, wires, and waveguides

In this section, we address charge transport. We particularly emphasize the possibility of designing tunable graphene-based charge-transporting elements. Unlike quantum dots (Section 5), where electrons are bound in a closed space, in graphene-based quantum wires and waveguides the charged particles should be confined only in *one* direction and be freely propagating in another one, as in *pnp*-structures.

There are several methods of charge confinement in graphene (see Sections 4–6 above). Typically, this is achieved either (i) chemically (by binding graphene atoms to foreign atoms: e.g., oxygen [201], fluoride [68,71,72], hydrogen [72,202], or aryl groups [73]); (ii) mechanically (either cutting or bending graphene sheets [162,203,204], or by creating inhomogeneous spatial strain distributions [23,204–206]); (iii) thermally [12], and (iv) electronically (by applying electromagnetic fields).

Each of these methods has its advantages and disadvantages. The first two are very effective; however, they are rather difficult to control, in the sense that any tuning (change of parameters) requires a reconstruction, either chemical or geometrical, of the whole graphene sample, which usually cannot be done quickly. Thus, these methods are not very suitable in designing *tunable* electronic devices.

Here we concentrate on confining electrons using electromagnetic fields. This approach is more flexible than chemical and mechanical approaches. Not only electromagnetic fields are easy to control, but being tailored properly, they enable the creation of graphene-based tunable elements, including quantum wires and waveguides with unique properties, such as unidirectional conductivity, robustness to disorder, etc. The diversity of methods and approaches makes it increasingly difficult to summarize the current state-of-the-art in this area, and calls for a systematic classification by both methods and results. An attempt of such classification is a goal of this chapter.

Manipulating charge carriers by *electric fields* (i.e., adding scalar potentials of different shapes to the Dirac equation) is a very popular approach (see, e.g., the reviews in Refs. [2,207]). This method has provided interesting and surprising outcomes (i.e., [4,207–209]). Unfortunately, it turned out to be impossible to repel or localize electrons in all directions and at all energies by only using an electric field [8]. There is always a channel in any electric-field barrier where the charge can escape through.

The charge-confining and current-guiding capabilities produced by *magnetic barriers* are well known and have already opened certain possibilities for practical applications (e.g., [210]). However, when it comes to designing fast-tunable electronic devices (switches, filters, etc.) a difficulty emerges: most of the existing magnetic-barrier technologies usually involve the deposition, either on top or beneath the graphene sheet, of a pattern of magnetic material, which reproduces the desired magnetic field distribution in the sample. Any subsequent change of parameters would require building a new setup, creating formidable (if surmountable) obstacles for harnessing magnetic barriers as elements of fast-acting electronic devices. Graphene structures based on the effective magnetic field created by applying inhomogeneous pressure or strain to the graphene sheet [204–206] might also be useful for applications.

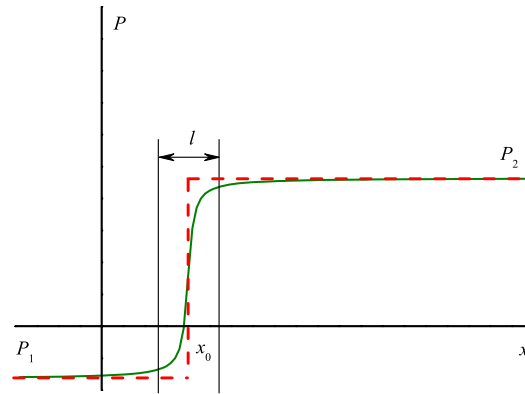


Fig. 25. (Color online) Depending on the problem being considered in this section, the function $P(x)$ is either one of the potentials $V(x)$, $A(x)$, or the magnetic field $B(x)$. Here, $P(x)$ is shown as a continuous green line, while the red dashed line repeats the step-like approximation.

An efficient way around this problem is the simultaneous use of inhomogeneous magnetic and electric fields. The proper combination of these two not only preserves (or even improves) the necessary transport properties of graphene samples, but makes them easy to control by tuning the spatial distribution of the electric potential, for a fixed magnetic field.

Hereafter, we focus on low-energy excitations when the inter-valley scattering [211] is negligible and quasiparticles can be considered as massless Dirac fermions. To simplify the presentation, all spin-related effects are also neglected below.

The building block of all charge-confining elements is a field-induced barrier (i.e., a reflecting wall). To introduce this in the most general way, consider two graphene half-planes, $x < x_0 - l/2$ and $x > x_0 + l/2$, subject to different stationary electric V_i and magnetic \mathbf{A}_i potentials ($i = 1, 2$), as shown in Fig. 25. Here we assume that $\mathbf{A} \equiv A(x)\hat{y}$, which means that the magnetic field $\mathbf{B} = B(x)\hat{z}$. When $|x - x_0| < l/2$, the fields and potentials are x -dependent, providing the transition from $\{V_1, A_1, \mathbf{B}_1\}$ to $\{V_2, A_2, \mathbf{B}_2\}$ (see Fig. 25). If the width l is large, compared to the graphene lattice spacing a , and much smaller than the Fermi wavelength λ_F , $a \ll l \ll \lambda_F$, then the smooth profile can be replaced in the calculations by a step function as shown by the dotted line in Fig. 25. When $B = 0$ we have pn junction, which is discussed in Section 6.

7.1. Magnetic barriers: $B \neq 0, V = 0$

As it was demonstrated theoretically in Refs. [150,212,213], charge carriers in graphene could be confined in space by applying a properly tailored static inhomogeneous magnetic field perpendicular to the graphene plane (x, y). There are numerous unusual and intriguing features in this phenomenon, but at its basic level, this happens because the trajectory of the quasiparticle incoming from free space $x < 0$ bends inside the magnetic barrier (Fig. 25) and eventually exits backward, independently of its cyclotron radius, thus making the wall a perfect reflector for Dirac electrons of any energy [214]. Obviously, a barrier of finite width reflects only charges with energies below a threshold, namely those whose cyclotron radius is smaller than d . Below we consider two types of these magnetic barriers.

7.1.1. Step-wise vector potential A : δ -function-like magnetic field B

This basic magnetic field profile, $B(x) = B_0 \ell_{B_0} \delta(x)$ (here $\ell_{B_0} = \sqrt{\hbar c / e B_0}$ is the magnetic length), already displays an important advantage of magnetic barriers over electric ones: there is a range of energies for which it is a perfect mirror for Dirac electrons for all angles of incidence including perpendicular [210]. Outside this energy range, the transparency is angular-dependent, and the analog of the total internal reflection (TIR) of light takes place when the angle of incidence exceeds some critical angle ϕ_{TIR} , which depends on the applied magnetic field. The resulting charge refraction is not of the classical Snell's law type, and is asymmetric with respect to the transformation of the angle of incidence $\phi \rightarrow -\phi$ [210].

Rather counter-intuitive is also the fact that a magnetic field, $B(x) \propto \delta(x)$, creates a bound (in the x -direction) state at zero energy. This state is a “linear” analog of two-dimensional surface waves: it is exponentially localized in the x -direction around the line $x = 0$, and propagates along the y -axis with wave numbers $\pm k_y$. The longitudinal wave number k_y is enclosed in the finite interval $(-\ell_{B_0}^{-1}/2, \ell_{B_0}^{-1}/2)$, and the x -dependence of the wave function is asymmetric, so that the rates of the exponential decay at $x < 0$ and $x > 0$ are different, depending on the sign of k_y (direction of propagation) [214]. The possibilities to experimentally produce highly localized magnetic fields have been discussed in Ref. [210], where charge transport in the presence of various arrangements of δ -type magnetic barriers was studied in terms of “electron optics”.

7.1.2. Step-wise magnetic field B : piece-wise linear vector potential A

The transport properties of Dirac electrons in a step-wise magnetic field [i.e., $B(x) = B_1\theta(-x) + B_2\theta(x)$] are different and of greater variety than in the step-wise potential considered in Section 7.1.1. While in the later case, the system is obviously invariant with respect to a shift of the A -step [namely, $A(x) \rightarrow A(x) + \text{const}$], for a step-wise B this is not true: B_1 and B_2 are parallel ($\gamma = B_1/B_2 > 0$) or antiparallel ($\gamma < 0$) makes a significant difference.

To better understand the behavior of Dirac electrons in nonhomogeneous magnetic fields, it is illuminating to compare it with the conventional two-dimensional electron gas. Fundamental differences already exist in the uniform field. In contrast with the classical Landau levels ε_n in infinite space, $\varepsilon_n \propto (n + 1/2)$, $n \geq 0$, the quantization of the eigen-energy of the Dirac equation produces $\varepsilon_n \propto \text{sign}(n)\sqrt{|n|}$, with $-\infty \leq n \leq \infty$. Positive values of n , $n > 0$, are associated with electron-like charge carriers, while $n < 0$ corresponds to holes. The eigenstates with $n \neq 0$ are similar to the states of the conventional two-dimensional electron gas, whereas the zero-energy state $n = 0$ possesses different properties. Bound states associated with this $n = 0$ Landau level have different features than the states associated with $n \neq 0$.

The energy in homogeneous magnetic fields does not depend on the wavenumber k , therefore the group velocity is zero, $v_g = d\varepsilon_n/dk = 0$, and the states carry no current. A dispersion, and therefore a non-zero group velocity $v_y = d\varepsilon_n/dk_y \neq 0$ can appear either for states localized near the boundary of a finite sample (so-called edge states), or due to the spatial inhomogeneity of the magnetic field, $\nabla_x B \neq 0$, which creates bound states localized in the x -direction and propagating along the y -axis with its drift velocity proportional to $\nabla B \times \mathbf{B}$ (denoted, by analogy with edge states, as *magnetic edge states* [215]).

For the particular case $B_1 = 0$ (free half-space for $x < 0$, constant magnetic field $B_2 > 0$ at $x > 0$), there is an infinite number of bound (in the x -direction) dispersive states labeled by the Landau-level index n , whose energies are proportional to $\text{sign}(n)\sqrt{|n|}$. These states are localized as functions of x , centered around points whose locations depend on the wave number k_y . Remarkably, these localized states exist only with one sign of the wave number k_y , either positive or negative, depending on the orientation of the magnetic field B_2 . Since the group velocity has opposite signs for $+n$ and $-n$, the direction of the charge flow created by electrons and holes is the same, and therefore any bound n -state carries a finite unidirectional current along the y -axis [210]. Therefore, a particle in such a state never undergoes backscattering; hence it is practically insensitive to disorder and Anderson localization never takes place, no matter how strong the disorder is. There is also a bound state with $\varepsilon = 0$, when $k_x = ik_y$. However, this state is dispersionless and does not carry any current.

When $B_1 \neq 0$ [216] and it is parallel with B_2 ($\gamma > 0$), the Landau levels of Dirac quasiparticles at large positive k_y are localized in an effective potential well around $x = -k_y \ell_B^2$. With k_y decreasing to negative values, the dimensionless energy levels gradually change to $\text{sign}(n)\sqrt{\gamma|n|}$ at large negative n and shift in space to $x = -k_y \ell_B^2/\gamma$. It is important to note that the directions of the drift (signs of $d\varepsilon_n/dk_y$) are opposite for electron- and hole-like particles ($\pm n$), thus providing a non-zero total current. In the vicinity of $k_y = 0$, the corresponding states become localized at $x = 0$. Similarly to $B_1 = 0$ case, the magnetic barrier with $\gamma > 0$ supports bound states, which create unidirectional conductivity at $n \neq 0$, while zero-energy solutions carry no currents.

When $\gamma < 0$ (for antiparallel B_1 and B_2) [216], the effective potential at large positive k_y has two minima (two coupled harmonic wells), located far away from the boundary $x = 0$, so that the states are localized in each well. As k_y moves to negative values, the effective potential shifts toward $x = 0$ and transforms into a single non-harmonic potential well. The eigen-energies with $n \neq 0$ correspond to states which support non-zero unidirectional current following classical, so-called snake, orbits [215] confined to a narrow one-dimensional channel centered at the line $x = 0$ where the magnetic field changes its sign. It was shown in Refs. [217,218] that in a symmetric graphene sample of a finite width L ($-L/2 \leq x \leq L/2$) this current is compensated by real edge states localized close to the sample boundaries. The states with $n = 0$ exhibit both electron and hole features, which is highly unusual and is unique for Dirac quasi-particles in graphene.

7.2. Combined magneto-electric barriers: $B \neq 0$, $V \neq 0$

In principle, the charge-confining and guiding capabilities of magnetic walls presented above open up certain possibilities for practical applications. However, as it was mentioned before, the parameters of the magnetic barriers cannot be changed fast enough, which makes it problematic to use them as elements of fast-acting electronic devices.

To overcome this problem, it is convenient to use a combination of inhomogeneous magnetic and electric fields, which enables the efficient control of the transport properties of graphene samples by tuning the electric potential without changing the parameters of the magnetic field.

To introduce a basic setup combining magnetic and electric fields, we now consider a single magneto-electric barrier produced by superimposing a scalar potential V of the same step-like shape on the magnetic structure with a δ -like magnetic field [i.e., a step-wise vector potential $A(x) = A_1\theta(-x) + A_2\theta(x)$]. This system possesses unique properties that make it different from other types of barriers. Graphene subject to mutually perpendicular electric and magnetic fields supports states which are localized near the barrier. These current-carrying states (surface waves) correspond to quasiparticles moving along the barrier only in one direction [219]. This direction, as well as the value of the quasiparticle velocity, are easily controlled by the electrostatic potential. These states correspond to the classical drift of charged particles in crossed electric and magnetic fields. They exist if and only if the drift velocity $v_d = cE/B$ is smaller than the Fermi velocity v_F [here $E \simeq (V_2 - V_1)/l$ and $B \simeq (A_1 - A_2)/l$ are the electric and magnetic fields in a barrier of finite length l]. The absence of counter-propagating states prevents the backscattering induced by either irregularities in graphene [188,208] or by the fluctuations of the magnetic field.

For potential applications, the important feature of a single magneto-electric barrier is that the transport (electric current) across or along this structure can be controlled by manipulating only the electric potentials V_1 and V_2 . In particular:

- The transmission and reflection coefficients across the junction between two areas with different values V_1 , A_1 and V_2 , A_2 (Fig. 25), and the angle of refraction (i.e., the direction of the transmitted current) depend on the electric potentials.

Specifically, tuning V_1 and/or V_2 can change the angle of incidence at which the barrier is totally transparent, and thus the Klein tunneling can be observed;

– When the inequality

$$|V_1 - \varepsilon| + |V_2 - \varepsilon| < |A_1 - A_2| \quad (5)$$

holds (here ε is the energy of the quasiparticles; all units are dimensionless), the step is a perfect reflector for electrons at all angles of incidence and the junction is locked for the electric current.

– If

$$|V_1 - V_2| < |A_1 - A_2|, \quad (6)$$

a wave (current) exists which propagates unidirectionally along the barrier (in the y -direction) with the dimensionless group velocity $\nu = v_d/v_F < 1$ and is exponentially localized in the x -direction.

7.3. Waveguide with electrically-tuned parameters

While one barrier forms a wire, two such barriers constitute a waveguide. This waveguide supports modes that are similar to the electromagnetic eigenmodes of a dielectric waveguide and likewise have quantized transverse wave numbers (The analogy between the transport of Dirac electrons in graphene and light propagation in dielectrics is described in Refs. [179,188,199,219]). However, along with them there is another set of waves that is appropriate to call “extraordinary” [219]. They are formed by two coupled surface waves propagating along the waveguide walls (barriers). There is an energy gap where only extraordinary modes exist. Decreasing the spacing between the barriers broadens this gap. The extraordinary modes are also stable against backscattering.

An important feature of field-induced waveguides in graphene, which is favorable for the creation of tunable electronic devices is that the transport properties of these structures are strongly dependent on the parameters of the barriers. These parameters are the potentials $A_{l,r}$ and $V_{l,r}$ of the left and right semiplanes, respectively, surrounding the central region where the potentials are equal to zero, $A_c = V_c = 0$. In particular:

– When

$$A_l = A_r \quad \text{and} \quad V_l = V_r$$

and the inequalities (5) and (6) are valid for both barriers (waveguide walls), then the extraordinary modes are unidirectional. This makes them immune to backscattering, and therefore robust against y -dependent disorder.

– If

$$A_l = -A_r \quad \text{and} \quad V_l = V_r,$$

then the surface waves “attached” to the barriers propagate along the y -axis in opposite directions and the extraordinary modes are bidirectional. Nevertheless, the backscattering also does not affect the total current, due to the spatial separation of the charge fluxes with opposite directions.

– When

$$A_l = -A_r \quad \text{and} \quad V_l = -V_r,$$

the spectrum of the extraordinary modes is independent of the distance between the barriers, and therefore there is no cutoff energy for them. This means that extraordinary modes can penetrate through an *arbitrary* narrow part of the waveguide.

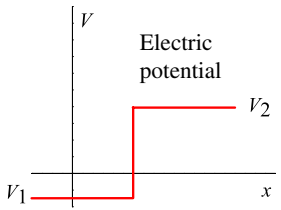
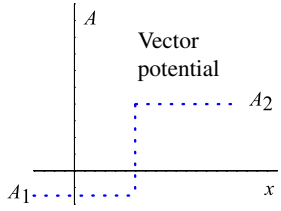
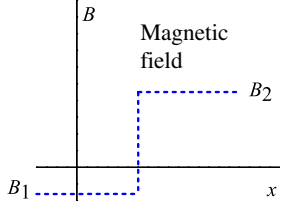
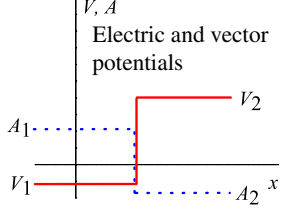
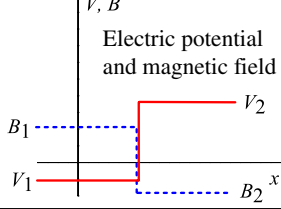
In Tables 10 and 11, the barriers and waveguides of the above mentioned types and combinations of fields are categorized according to the following features:

- Their ability to reflect all incident current (perfect wall)
- Their ability to support bound electron states
- The type of spectrum of the propagating modes (either continuous or discrete)
- The directionality of the current (either uni- or in bidirectional)
- A separate column lists some other distinctive features because graphene in magnetic fields has unusual properties.

In summary, changing the electric potential (with the magnetic field unchanged) one can switch on and off the current through the barrier and create/destroy a unidirectional quantum wire along the barrier. Moreover, changing the electric potential one can create waveguides with unique, exotic transport properties.

Table 10

Basic properties of electric and/or magnetic barriers in graphene. The ability to reflect all incident electric currents (or the ability to be a perfect reflecting wall) is indicated in the second column. The presence or absence of bound states is listed in the third column. Additional physical properties are summarized in the remaining columns.

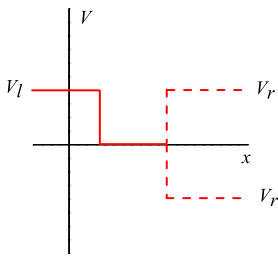
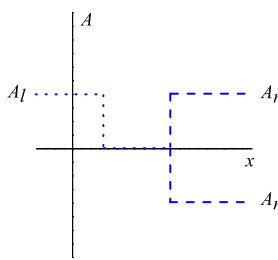
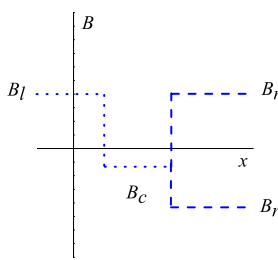
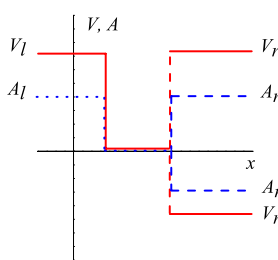
Barrier type	Perfect wall	Bound states	Directionality of the bound state current	Comments
 <p>Electric potential</p>	No	No	No bound state current.	When $\min\{V_i\} < \mathcal{E} < \max\{V_i\}$, the optics analogy of the barrier is the interface between two dielectrics with opposite signs of the refraction indices. Otherwise, this is the interface between usual dielectric media. Total internal refraction is possible. Cannot be opaque for all angles of incidence (i.e., Klein tunneling).
 <p>Vector potential</p>	Yes	Yes	One bound state with zero energy ($\mathcal{E} = 0$) and zero group velocity ($v_g = 0$) along the barrier, and, therefore, carries no current. This bound state is associated with the Landau level with $n = 0$.	In a certain range of energies the barrier is opaque for all angles of incidence. This barrier is similar to the barrier generated by a graphene sheet strain. The difference is that the strain generates an effective vector potentials jump (effective magnetic fields) with opposite (due to the time-reversal symmetry) signs in two valleys, whereas the real magnetic field has the same sign in both valleys.
 <p>Magnetic field</p>	Yes	Yes	Bi-directional conductivity when both B_1 and B_2 are non-zero; otherwise uni-directional conductivity along the barrier.	When $\gamma = B_1/B_2 > 0$, the bound state is similar to the classical electrodynamics state with $\nabla B \times \vec{B}$ drift. When $\gamma < 0$ and Landau-level index $n \neq 0$, the state is similar to a snake state (charged particle motion along the $B = 0$ line). Can be opaque for all angles of incidence.
 <p>Electric and vector potentials</p>	Yes	Yes	Confined uni-directional state with linear spectrum $d\mathcal{E}/dk_y = v_d$ when $ v_d = c (V_2 - V_1)/(A_1 - A_2) < v_F$. In a certain range of energies, the barrier is opaque for all angles of incidence. Easily controlled by the electric potential.	The classical electrodynamics analogy of the bound state is the charged particle drift in crossed electric and magnetic fields. The drift velocity is $v_d = cE/B = c(V_2 - V_1)/(A_1 - A_2)$
 <p>Electric potential and magnetic field</p>	Yes	Yes	Same as the magnetic field barrier shown above.	Same as the magnetic field barrier shown above.

8. Conclusions

Graphene is a material with many interesting features which makes it an attractive candidate for microelectronic and micromechanical applications. In the above pages we very briefly outlined several ideas and notions driving current graphene mesoscopic research: edge states, geometric quantization, quasi-bound states, Coulomb blockade, Klein tunneling through pn -junctions, etc. Some of them, like Klein tunneling, are unique to graphene. Others, e.g., Coulomb blockade and geometric quantization, have a much longer history. Yet, even in the latter case, the peculiar properties of graphene give rise to new features, for example, a much larger energy scale for the confinement inside a quantum dot.

Table 11

Basic properties of waveguides in graphene. These are produced by various configurations of the applied electric and magnetic fields. Note that the convention used here for dotted and dashed lines is different from the one used in Table 10.

Waveguide type	Guided modes	Comments
	Discrete set of bulk waves.	Optics analogy: this is a dielectric waveguide based on total internal reflection.
	Discrete set of bulk waves and one surface mode with zero group velocity along the waveguide.	The bulk waves are similar to dielectric waveguide modes. The surface mode is localized near the waveguide walls and consists of two coupled surface modes associated with the barriers (the waveguide walls).
	Discrete set of bulk waves when $\sigma = B_l/B_r = \pm 1$ and $B_c = 0$. The mode is localized near the boundaries when $\sigma = 1$ and $B_c < 0$.	The discrete set of bulk waves is similar to the eigenmodes of a dielectric slab surrounded by a medium with negative permittivity/permeability. It always has a snake state with noncompensated current. When $\sigma = 1$ and $B_c < 0$, there are counter-propagating currents near the walls (two snake states near the walls).
	Discrete set of bulk waves and two surface modes.	Bulk waves are similar to the eigenmodes of dielectric waveguides. When the spacing between the barriers is rather small, there are only surface modes. The propagation direction of surface modes is controlled by the electric potentials.

Although, many of the theoretical studies of graphene mesoscopic systems are done in the single-electron approximation, the use of many-body techniques are often warranted. Indeed, the single-electron approximation could introduce qualitative errors, which may be corrected only if proper many-body effects are accounted.

Numerous theoretical proposals have not been explored experimentally. For instance, the realization of nanoribbons with atomically-sharp edges remains a distant possibility. Many suggested devices impose stringent conditions on samples, in terms of purity and regularity of the sample's geometry. Some of these proposals are stimulating various current experiments. An important direction in this quest is to control and to understand the disorder, which may enter through many routes: as foreign atoms adsorbed on samples or chemically attached to the edges, as imperfections of the sample edges, as random elastic deformations, or as bulk defects of varied nature. On the other hand, disorder is not always an enemy, since its use may be beneficial under certain circumstances.

Graphene studies are still in their infancy, and it is too early to guess which of its unusual features will be more useful for applications. Yet, fabrication of several prototypic microelectronic devices, like field-effect transistors, biosensors, and integrated circuits, have been reported. In addition, graphene presents an excellent playground for fundamental condensed

matter research, exciting enthusiasm of both experimentalists and theorists in numerous subfields of condensed matter physics.

Acknowledgements

We are grateful to L.A. Openov who provided a high-resolution file used to create Fig. 6. We are grateful for the support provided by the grant RFBR-JSPS 09-02-92114. A.V.R. is partially supported by the grant RFBR 09-02-00248. G.G. acknowledges support from the Japan Society for the Promotion of Science (JSPS). F.N. acknowledges partial support from the National Security Agency (NSA), Laboratory Physical Sciences (LPS), Army Research Office (ARO), DARPA, Air Force Office of Scientific Research (AFOSR), and National Science Foundation (NSF) grant No. 0726909, Grant-in-Aid for Scientific Research (S), MEXT Kakenhi on Quantum Cybernetics, and Funding Program for Innovative R&D on S&T (FIRST).

Appendix A. Tight-binding model of graphene lattice

In this appendix we present basic notions necessary for the theoretical description of the single-electron properties of a graphene sheet. It provides some details omitted in Section 2.

It is common to describe a graphene sample in terms of a tight-binding model on the honeycomb lattice. Such lattice can be split into two sublattices, denoted by \mathcal{A} and \mathcal{B} . The Hamiltonian of an electron hopping on the graphene sheet is given by Eq. (1), in which \mathbf{R} runs over sublattice \mathcal{A}

$$\mathbf{R} = \delta_1 + \mathbf{a}_1 n_1 + \mathbf{a}_2 n_2, \quad (\text{A.1})$$

where the primitive vectors of the honeycomb lattice are

$$\mathbf{a}_1 = a_0(3/2, \sqrt{3}/2), \quad (\text{A.2})$$

$$\mathbf{a}_2 = a_0(3/2, -\sqrt{3}/2), \quad (\text{A.3})$$

and $n_{1,2}$ are integers. The vectors δ_i ($i = 1, 2, 3$) connect the nearest neighbors. They are

$$\delta_1 = a_0(-1, 0), \quad (\text{A.4})$$

$$\delta_2 = a_0(1/2, \sqrt{3}/2), \quad (\text{A.5})$$

$$\delta_3 = a_0(1/2, -\sqrt{3}/2). \quad (\text{A.6})$$

The geometry of the graphene lattice is presented in Fig. 1.

The Schrödinger equation can be written as

$$\varepsilon \psi_{\mathbf{R}}^{\mathcal{A}} = -t \psi_{\mathbf{R}+\delta_1}^{\mathcal{B}} - t \sum_{i=1,2} \psi_{\mathbf{R}+\delta_1+\mathbf{a}_i}^{\mathcal{B}}, \quad (\text{A.7})$$

$$\varepsilon \psi_{\mathbf{R}+\delta_1}^{\mathcal{B}} = -t \psi_{\mathbf{R}}^{\mathcal{A}} - t \sum_{i=1,2} \psi_{\mathbf{R}-\mathbf{a}_i}^{\mathcal{A}}, \quad (\text{A.8})$$

where $\psi_{\mathbf{R}}^{\mathcal{A}}$ ($\psi_{\mathbf{R}+\delta_1}^{\mathcal{B}}$) denotes the wave function value at the site \mathbf{R} (at the site $\mathbf{R} + \delta_1$) of sublattice \mathcal{A} (sublattice \mathcal{B}).

The primitive cell of graphene contains two atoms, one at \mathbf{R} , another at $\mathbf{R} + \delta_1$. Therefore, it is convenient to define the two-component (spinor) wave function

$$\Psi_{\mathbf{R}} = \begin{pmatrix} \psi_{\mathbf{R}}^{\mathcal{A}} \\ \psi_{\mathbf{R}+\delta_1}^{\mathcal{B}} \end{pmatrix}. \quad (\text{A.9})$$

By construction, the function $\Psi_{\mathbf{R}}$ is defined on sublattice \mathcal{A} , Eq. (A.1).

The action of H on a plane wave

$$\Psi_{\mathbf{R}} = \Psi_{\mathbf{k}} \exp(-i\mathbf{k} \cdot \mathbf{R}) \quad (\text{A.10})$$

can be expressed as

$$H\Psi_{\mathbf{k}} = \begin{pmatrix} 0 & -t_{\mathbf{k}} \\ -t_{\mathbf{k}}^* & 0 \end{pmatrix} \Psi_{\mathbf{k}}, \quad (\text{A.11})$$

$$t_{\mathbf{k}} = t \left[1 + 2 \exp\left(-i\frac{3k_x a_0}{2}\right) \cos\left(\frac{\sqrt{3}}{2} k_y a_0\right) \right]. \quad (\text{A.12})$$

For every \mathbf{k} there are two eigenstates

$$\Psi_{\mathbf{k}\pm} = \begin{pmatrix} 1 \\ \mp e^{-i\theta_{\mathbf{k}}} \end{pmatrix}, \quad (\text{A.13})$$

$$\exp(i\theta_{\mathbf{k}}) = \frac{t_{\mathbf{k}}}{|t_{\mathbf{k}}|}, \quad (\text{A.14})$$

with eigenvalues:

$$\varepsilon_{\mathbf{k}\pm} = \pm |t_{\mathbf{k}}| = \pm t \sqrt{3 + F(\mathbf{k})}, \quad (\text{A.15})$$

$$F(\mathbf{k}) = 4 \cos\left(\frac{3}{2}k_x a_0\right) \cos\left(\frac{\sqrt{3}}{2}k_y a_0\right) + 2 \cos\left(\sqrt{3}k_y a_0\right). \quad (\text{A.16})$$

The states with negative (positive) energy are filled (empty) at $T = 0$. The allowed values of \mathbf{k} lie within the Brillouin zone presented in Fig. 2.

The reciprocal lattice is characterized by the following lattice vectors

$$\mathbf{d}_1 = (4\pi/3a_0, 0), \quad (\text{A.17})$$

$$\mathbf{d}_2 = (-2\pi/3a_0, 2\pi/\sqrt{3}a_0). \quad (\text{A.18})$$

The amplitude $t_{\mathbf{k}}$ and energy $\varepsilon_{\mathbf{k}\pm}$ are invariant under shifts over $\mathbf{d}_{1,2}$.

The quantity $\varepsilon_{\mathbf{k}\pm}$ vanishes at the six corners of the Brillouin zone: $\mathbf{K}_{1,2} = (0, \pm 4\pi/(3\sqrt{3}a_0))$ and $\mathbf{K}_{3,4,5,6} = (\pm 2\pi/(3a_0), \pm 2\pi/(3\sqrt{3}a_0))$. These are the locations of the famous Dirac cones of graphene. These six cones can be split into two equivalence classes: all cones inside a given equivalence class are connected by reciprocal vectors. We choose cones located at $\mathbf{K}_{1,2}$ to be representatives of these classes.

If one is interested in the low-energy description only, then the tight-binding Hamiltonian may be replaced by the Dirac Hamiltonian with the help of the following derivation. Near the cones, the Hamiltonian equation (A.11) may be expanded in orders of $\mathbf{k} - \mathbf{K}_{1,2}$. The spinor itself may be represented as

$$\Psi(\mathbf{R}) = \Psi_1(\mathbf{R}) \exp(-i\mathbf{K}_1 \cdot \mathbf{R}) + \Psi_2(\mathbf{R}) \exp(-i\mathbf{K}_2 \cdot \mathbf{R}), \quad (\text{A.19})$$

and the Schrödinger equation splits into two copies of the Weyl–Dirac equation (3), where we treat $\Psi_{1,2}(\mathbf{R})$ as slowly varying functions of the continuous variable \mathbf{R} , and the plus (minus) sign is chosen for Ψ_1 (Ψ_2).

Describing the electronic properties of the graphene in terms of Eq. (3) is very popular for two reasons. First, it is much simpler than the full tight-binding Hamiltonian (1). Second, unlike the tight-binding Hamiltonian, which may require knowledge of several hopping amplitudes, only one parameter v_F has to be specified. Of course, the tight-binding model is needed when a more detailed description is required.

Appendix B. Edge states

Usually, two types of edges are discussed in the literature: zigzag and armchair. A variant of the zigzag is the Klein edge [33]. All three types are shown in Fig. 1.

B.1. Armchair edge

The physics of the armchair edge is simpler than that of the zigzag edge because the latter supports zero-energy localized states, while the former does not. The easiest way to describe an electron near an armchair edge is to use the Weyl–Dirac equation (3) with the appropriate boundary condition. The general problem of the boundary condition for the Weyl–Dirac equation was investigated in Refs. [34,36,50–52]. Here we use a simple explicit form of the boundary condition suitable for armchair edge [81]. Namely, we demand that our spinor wave function (Eq. (A.19)) vanishes at the edge, which we assume to be located at $y = 0$

$$\Psi_1(\mathbf{R})|_{y=0} = -\Psi_2(\mathbf{R})|_{y=0}. \quad (\text{B.1})$$

For an infinite half-plane, the solution of the Weyl–Dirac equations with this boundary condition is equal to

$$\Psi_{1\pm}(\mathbf{R}) = \frac{1}{\sqrt{2}} \begin{pmatrix} 1 \\ \mp (ik_x + k_y)/k \end{pmatrix} \exp(-ik_x x - ik_y y), \quad (\text{B.2})$$

$$\Psi_{2\pm}(\mathbf{R}) = -\frac{1}{\sqrt{2}} \begin{pmatrix} 1 \\ \mp (ik_x + k_y)/k \end{pmatrix} \exp(-ik_x x + ik_y y). \quad (\text{B.3})$$

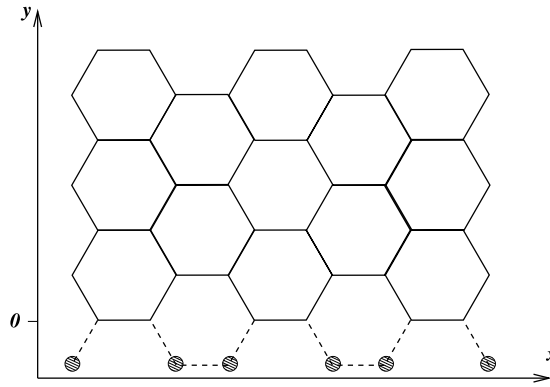


Fig. 26. Introduction of auxiliary atoms (hatched circles) at an armchair edge.

The eigenfunctions $\Psi_{1,2+}$ ($\Psi_{1,2-}$) correspond to positive (negative) eigenvalues. The total wave function is to be constructed according to Eq. (A.19).

However, it is not necessary to use the approximate description in terms of the Weyl–Dirac equation. The tight-binding model may be solved near the armchair edge as well. To construct such a solution, note first that the atoms at the very edge are special: they have only two nearest neighbors, while the atoms in the bulk have three. This means that Eqs. (A.7) and (A.8) must be modified to account for this fact. It is more convenient, however, to introduce auxiliary rows of carbon atoms (Fig. 26) and demand that the wave function vanishes on these additional atoms. Since there is no wave function density on the auxiliary atoms, they do not contribute to the Schrödinger equation for the physical atoms at the edge. This construction is used in several papers (e.g., Refs. [88,90]). The solution of Eqs. (A.7) and (A.8) is

$$\Psi_{\mathbf{R}} = \Psi_{\mathbf{k}\pm} \exp(-ik_x x) \sin[k_y (y + \sqrt{3}a_0/2)]. \quad (\text{B.4})$$

This wave function vanishes at $y = -\sqrt{3}a_0/2$, which is where the auxiliary atoms are located. At the physical edge of the nanoribbon ($y = 0$), however, the electron density remains non-zero. Note that momentum components $k_{x,y}$ in Eq. (B.4) is measured from the center of the Brillouin zone. However, in Eqs. (B.2) and (B.3) they are measured from the Dirac cones. When this subtlety is accounted it is easy to demonstrate that both solutions have the identical dependence on \mathbf{R} . They differ only in the value of the spinor part $\Psi_{\mathbf{k}}$. This is because Eqs. (B.2) and (B.3) are only approximations which are accurate at small energy only.

The discussion presented above assumes that the properties of the carbon–carbon bonds near the edge remain the same. In a real sample this assumption is only an approximation. A variety of perturbations may be present near the edge. For example, Ref. [220] investigated the edge structure with the help of density-functional methods. It was found that the carbon–carbon bonds at armchair edges are shorter than in the bulk (1.26 Å versus 1.4 Å). This means that the effective electron hopping at the edge t_e differs from its value t in the bulk.

Also, non-carbon radicals may be attached to the unpaired chemical bond of carbon atoms at the armchair edge. This means that, depending on the description, either the Hamiltonian near the edge, or the boundary conditions have to be modified. Fortunately, these alterations are small, and may be treated as weak corrections.

B.2. Zigzag edge

The physics of the zigzag edge is richer than the physics of the armchair edge due to the zero-energy states localized at the edge. When graphene is described by the Hamiltonian (1), which only contains nearest-neighbor hopping, these states are dispersionless and macroscopically degenerate.

The easiest way to detect the presence of edge states is to use the Weyl–Dirac equation with the boundary condition appropriate for the zigzag edge [34,36,50]. For the purpose of demonstrating the presence of edge states the simplest version of the boundary condition is used here [81]. The zigzag edge, unlike the armchair edge, consists of atoms belonging to the same sublattice. This is clearly seen in Fig. 1: all atoms at the left edge belong to \mathcal{A} sublattice (red). The right zigzag edge has all its atoms on the \mathcal{B} sublattice. Extending the left edge by a column of the auxiliary atoms, we demand that the wave function vanishes on them (assume that the auxiliary atoms are located at $x = 0$):

$$\psi^{\mathcal{B}}|_{x=0} = 0. \quad (\text{B.5})$$

Then the following spinor functions are the solutions of the Weyl–Dirac equation: when $k_y > 0$

$$\Psi_1(\mathbf{R}) = \begin{pmatrix} 1 \\ 0 \end{pmatrix} \exp(-k_y x + ik_y y), \quad \Psi_2 = 0; \quad (\text{B.6})$$

and when $k_y < 0$

$$\psi_1 = 0, \quad \psi_2(\mathbf{R}) = \begin{pmatrix} 1 \\ 0 \end{pmatrix} \exp(-|k_y|x + ik_y y). \quad (\text{B.7})$$

Both solutions decay for large values of x and correspond to the zero eigenenergy. The difference between them is that Eq. (B.6) describes the solution near \mathbf{K}_1 , while Eq. (B.7) near \mathbf{K}_2 . The wave function Eq. (A.19) constructed from Eqs. (B.6) and (B.7) is equal to

$$\Psi(\mathbf{R}) = a \begin{pmatrix} 1 \\ 0 \end{pmatrix} \exp(-i\mathbf{K}_1 \cdot \mathbf{R} - k_y x + ik_y y) + b \begin{pmatrix} 1 \\ 0 \end{pmatrix} \exp(-i\mathbf{K}_2 \cdot \mathbf{R} - k'_y x - ik'_y y), \quad (\text{B.8})$$

where both k_y and k'_y are positive and small compared to $1/a_0$. The quantity k_y sets a parameter with dimension of length

$$\lambda_{\text{edge}} = \frac{1}{|k_y|} \quad (\text{B.9})$$

which characterizes how deeply the edge states extend into the bulk of graphene.

Since the Weyl–Dirac equation is only an approximation of the tight-binding Hamiltonian (1), we cannot reliably use Eq. (B.8) for large values of k_y and k'_y . However, the tight-binding problem may be solved exactly [35] to discover that there is a degenerate manifold of states labeled by the momentum k_y , which stretches from \mathbf{K}_1 to \mathbf{K}_2 .

B.2.1. Effect of the longer-range hopping

The degeneracy of edge states is purely accidental property of Hamiltonian (1). It disappears when other terms are added to H . For example, in Refs. [55–58] the effect of next-to-nearest-neighbor hopping on edge states was studied both analytically and numerically. In Ref. [58] the authors made three keen observations: (i) the next-to-nearest-neighbor hopping effectively induces a shift in the local potential; (ii) the shift depends on site's position, namely, near the edge it is not the same as in the bulk; and (iii) this spacial variation of the potential induces finite dispersion for otherwise dispersionless edge states. To prove that (iii) holds true, consider the following argument. The states with large λ_{edge} are insensitive to the potential variation (they “feel” the potential averaged over large λ_{edge}), however, those with small λ_{edge} are affected strongly; since λ_{edge} depends on $|k_y|$, the edge states acquire the dispersion.

This discussion suggests that, if we were to describe this phenomenon with the help of the Weyl–Dirac equation, the boundary conditions, Eq. (B.5), must be modified to account for the effect of the potential modulation near the boundary. Indeed, it was demonstrated in Ref. [52] that one can generalize Eq. (B.5) and reproduce the findings of Ref. [58], at least near the apexes of the Dirac cones.

References

- [1] A.K. Geim, K.S. Novoselov, The rise of graphene, *Nat. Mater.* 6 (2007) 183.
- [2] A.H. Castro Neto, F. Guinea, N.M.R. Peres, K.S. Novoselov, A.K. Geim, The electronic properties of graphene, *Rev. Modern Phys.* 81 (2009) 109.
- [3] K. Novoselov, A. Geim, S. Morozov, D. Jiang, Y. Zhang, S. Dubonos, I. Grigorieva, A. Firsov, Electric field effect in atomically thin carbon films, *Science* 306 (2004) 666.
- [4] D.S.L. Abergel, V. Apalkov, J. Berashevich, K. Ziegler, T. Chakraborty, Properties of graphene: a theoretical perspective, *Adv. Phys.* 59 (2010) 261.
- [5] M.J. Allen, V.C. Tung, R.B. Kaner, Honeycomb carbon: a review of graphene, *Chem. Rev.* 110 (2010) 132.
- [6] O.V. Yazyev, Emergence of magnetism in graphene materials and nanostructures, *Rep. Progr. Phys.* 73 (2010) 056501.
- [7] A. Cresti, N. Nemeč, B. Biel, G. Niebler, F. Triozon, G. Cuniberti, S. Roche, Charge transport in disordered graphene-based low dimensional materials, *Nano Res.* 1 (2008) 361.
- [8] C.W.J. Beenakker, Colloquium: Andreev reflection and Klein tunneling in graphene, *Rev. Modern Phys.* 80 (2008) 1337.
- [9] S. Das Sarma, S. Adam, E.H. Hwang, E. Rossi, Electronic transport in two dimensional graphene, <http://arxiv.org/abs/1003.4731>, 2010.
- [10] E.R. Mucciolo, C.H. Lewenkopf, Disorder and electronic transport in graphene, *J. Phys.: Condens. Matter* 22 (2010) 273201.
- [11] K.I. Bolotin, K.J. Sikes, J. Hone, H.L. Stormer, P. Kim, Temperature-dependent transport in suspended graphene, *Phys. Rev. Lett.* 101 (2008) 096802.
- [12] X. Du, I. Skachko, A. Barker, E.Y. Andrei, Approaching ballistic transport in suspended graphene, *Nat. Nano* 3 (2008) 491.
- [13] Y.M. Lin, C. Dimitrakopoulos, K.A. Jenkins, D.B. Farmer, H.Y. Chiu, A. Grill, P. Avouris, 100-GHz transistors from wafer-scale epitaxial graphene, *Science* 327 (2010) 662.
- [14] T.O. Wehling, K.S. Novoselov, S.V. Morozov, E.E. Vdovin, M.I. Katsnelson, A.K. Geim, A.I. Lichtenstein, Molecular doping of graphene, *Nano Lett.* 8 (2008) 173.
- [15] J.S. Bunch, A.M. van der Zande, S.S. Verbridge, I.W. Frank, D.M. Tanenbaum, J.M. Parpia, H.G. Craighead, P.L. McEuen, Electromechanical resonators from graphene sheets, *Science* 315 (2007) 490.
- [16] M.H.F. Sluiter, Y. Kawazoe, Cluster expansion method for adsorption: application to hydrogen chemisorption on graphene, *Phys. Rev. B* 68 (2003) 085410.
- [17] J.O. Sofo, A.S. Chaudhari, G.D. Barber, Graphene: a two-dimensional hydrocarbon, *Phys. Rev. B* 75 (2007) 153401.
- [18] M. Fujita, M. Igami, K. Nakada, Lattice distortion in nanographite ribbons, *J. Phys. Soc. Japan* 66 (1997) 1864.
- [19] M.Y. Han, B. Özyilmaz, Y. Zhang, P. Kim, Energy band-gap engineering of graphene nanoribbons, *Phys. Rev. Lett.* 98 (2007) 206805.
- [20] Z. Chen, Y.-M. Lin, M.J. Rooks, P. Avouris, Graphene nano-ribbon electronics, *Physica E* 40 (2007) 228.
- [21] J.L. McChesney, A. Bostwick, T. Ohta, T. Seyller, K. Horn, J. González, E. Rotenberg, Extended van Hove singularity and superconducting instability in doped graphene, *Phys. Rev. Lett.* 104 (2010) 136803.
- [22] Z.H. Ni, T. Yu, Y.H. Lu, Y.Y. Wang, Y.P. Feng, Z.X. Shen, Uniaxial strain on graphene: Raman spectroscopy study and band-gap opening, *ACS Nano* 2 (2008) 2301.
- [23] T. Low, F. Guinea, M.I. Katsnelson, Gaps tunable by gates in strained graphene, <http://arxiv.org/abs/1012.0939>, 2010.

- [24] R.M. Ribeiro, N.M.R. Peres, J. Coutinho, P.R. Briddon, Inducing energy gaps in monolayer and bilayer graphene: local density approximation calculations, *Phys. Rev. B* 78 (2008) 075442.
- [25] T. Ohta, A. Bostwick, T. Seyller, K. Horn, E. Rotenberg, Controlling the electronic structure of bilayer graphene, *Science* 313 (2006) 951.
- [26] Y.B. Zhang, T.T. Tang, C. Girit, Z. Hao, M.C. Martin, A. Zettl, M.F. Crommie, Y.R. Shen, F. Wang, Direct observation of a widely tunable bandgap in bilayer graphene, *Nature* 459 (2009) 820.
- [27] G. Giovannetti, P.A. Khomyakov, G. Brocks, P.J. Kelly, J. van den Brink, Substrate-induced band gap in graphene on hexagonal boron nitride: ab initio density functional calculations, *Phys. Rev. B* 76 (2007) 073103.
- [28] S.Y. Zhou, G.H. Gweon, A.V. Fedorov, P.N. First, W.A. De Heer, D.H. Lee, F. Guinea, A.H.C. Neto, A. Lanzara, Substrate-induced bandgap opening in epitaxial graphene, *Nat. Mater.* 6 (2007) 916.
- [29] R.P. Tiwari, D. Stroud, Tunable band gap in graphene with a noncentrosymmetric superlattice potential, *Phys. Rev. B* 79 (2009) 205435.
- [30] J. Berashevich, T. Chakraborty, Tunable band gap and magnetic ordering by adsorption of molecules on graphene, *Phys. Rev. B* 80 (2009) 033404.
- [31] B.N. Szafranek, D. Schall, M. Otto, D. Neumaier, H. Kurz, Electrical observation of a tunable band gap in bilayer graphene nanoribbons at room temperature, *Appl. Phys. Lett.* 96 (2010) 112103.
- [32] E.V. Castro, K.S. Novoselov, S.V. Morozov, N.M.R. Peres, J.M. B.L. Dos Santos, J. Nilsson, F. Guinea, A.K. Geim, A.H.C. Neto, Biased bilayer graphene: semiconductor with a gap tunable by the electric field effect, *Phys. Rev. Lett.* 99 (2007) 216802.
- [33] D. Klein, Graphitic polymer strips with edge states, *Chem. Phys. Lett.* 217 (1994) 261.
- [34] D.M. Basko, Boundary problems for Dirac electrons and edge-assisted Raman scattering in graphene, *Phys. Rev. B* 79 (2009) 205428.
- [35] K. Nakada, M. Fujita, G. Dresselhaus, M.S. Dresselhaus, Edge state in graphene ribbons: nanometer size effect and edge shape, *Phys. Rev. B* 54 (1996) 17954.
- [36] A.R. Akhmerov, C.W.J. Beenakker, Boundary conditions for Dirac fermions on a terminated honeycomb lattice, *Phys. Rev. B* 77 (2008) 085423.
- [37] G. Tkachov, Dirac fermion quantization on graphene edges: isospin-orbit coupling, zero modes, and spontaneous valley polarization, *Phys. Rev. B* 79 (2009) 045429.
- [38] C.K. Gan, D.J. Srolovitz, First-principles study of graphene edge properties and flake shapes, *Phys. Rev. B* 81 (2010) 125445.
- [39] P. Koskinen, S. Malola, H. Hakkinen, Self-passivating edge reconstructions of graphene, *Phys. Rev. Lett.* 101 (2008) 115502.
- [40] P. Koskinen, S. Malola, H. Hakkinen, Evidence for graphene edges beyond zigzag and armchair, *Phys. Rev. B* 80 (2009) 073401.
- [41] T. Wassmann, A.P. Seitsonen, A.M. Saitta, M. Lazzeri, F. Mauri, Structure, stability, edge states, and aromaticity of graphene ribbons, *Phys. Rev. Lett.* 101 (2008) 096402.
- [42] T. Wassmann, A.P. Seitsonen, A.M. Saitta, M. Lazzeri, F. Mauri, The thermodynamic stability and simulated STM images of graphene nanoribbons, *Phys. Status. Solidi. (B)* 246 (2009) 2586.
- [43] O. Volnianska, P. Boguslawski, Magnetism of solids resulting from spin polarization of p orbitals, *J. Phys. Condens. Matter.* 22 (2010) 073202.
- [44] K.A. Ritter, J.W. Lyding, The influence of edge structure on the electronic properties of graphene quantum dots and nanoribbons, *Nat. Mater.* 8 (2009) 235.
- [45] Ç.Ö. Girit, J.C. Meyer, R. Erni, M.D. Rossell, C. Kisielowski, L. Yang, C.-H. Park, M.F. Crommie, M.L. Cohen, S.G. Louie, et al., Graphene at the edge: stability and dynamics, *Science* 323 (2009) 1705.
- [46] T. Nakajima, K. Shintani, Molecular dynamics study of energetics of graphene flakes, *J. Appl. Phys.* 106 (2009) 114305.
- [47] E. Clar, Polycyclic Hydrocarbons, Academic Press, London, 1964.
- [48] E. Clar, The Aromatic Sextet, Wiley, New York, 1972.
- [49] C.D. Reddy, A. Ramasubramaniam, V.B. Shenoy, Y.-W. Zhang, Edge elastic properties of defect-free single-layer graphene sheets, *Appl. Phys. Lett.* 94 (2009) 101904.
- [50] E. McCann, V.I. Fal'ko, Symmetry of boundary conditions of the Dirac equation for electrons in carbon nanotubes, *J. Phys. Condens. Matter* 16 (2004) 2371.
- [51] V.A. Volkov, I.V. Zagorodnev, Electrons near a graphene edge, *Low Temp. Phys.* 35 (2009) 2.
- [52] V.A. Volkov, I.V. Zagorodnev, Electron states near graphene edge, *J. Phys. Conf. Ser.* 193 (2009) 012113.
- [53] Y. Niimi, T. Matsui, H. Kambara, K. Tagami, M. Tsukada, H. Fukuyama, Scanning tunneling microscopy and spectroscopy of the electronic local density of states of graphite surfaces near monoatomic step edges, *Phys. Rev. B* 73 (2006) 085421.
- [54] Y. Kobayashi, K.-i. Fukui, T. Enoki, K. Kusakabe, Y. Kaburagi, Observation of zigzag and armchair edges of graphite using scanning tunneling microscopy and spectroscopy, *Phys. Rev. B* 71 (2005) 193406.
- [55] N. Peres, F. Guinea, A. Neto, Electronic properties of disordered two-dimensional carbon, *Phys. Rev. B* 73 (2006) 125411.
- [56] K. Sasaki, S. Murakami, R. Saito, Stabilization mechanism of edge states in graphene, *Appl. Phys. Lett.* 88 (2006) 113110.
- [57] K.-i. Sasaki, S. Murakami, R. Saito, Gauge field for edge state in graphene, *J. Phys. Soc. Japan* 75 (2006) 074713.
- [58] K. Sasaki, Y. Shimomura, Y. Takane, K. Wakabayashi, Hamiltonian decomposition for bulk and surface states, *Phys. Rev. Lett.* 102 (2009) 146806.
- [59] K. Kusakabe, K. Wakabayashi, M. Igami, K. Nakada, M. Fujita, Magnetism of nanometer-scale graphite with edge or topological defects, *Mol. Cryst. Liq. Cryst. A* 305 (1997) 445.
- [60] O.V. Yazyev, M.I. Katsnelson, Magnetic correlations at graphene edges: basis for novel spintronics devices, *Phys. Rev. Lett.* 100 (2008) 047209.
- [61] H. Kumazaki, D.S. Hirashima, Local magnetic moment formation on edges of graphene, *J. Phys. Soc. Japan* 77 (2008) 044705.
- [62] K. Sasaki, R. Saito, Magnetism as a mass term of the edge states in graphene, *J. Phys. Soc. Japan* 77 (2008) 054703.
- [63] B. Wunsch, T. Stauber, F. Sols, F. Guinea, Interactions and magnetism in graphene boundary states, *Phys. Rev. Lett.* 101 (2008) 036803.
- [64] K. Sasaki, K. Sato, R. Saito, J. Jiang, Local density of states at zigzag edges of carbon nanotubes and graphene, *Phys. Rev. B* 75 (2007) 235430.
- [65] D.C. Elias, R.R. Nair, T.M.G. Mohiuddin, S.V. Morozov, P. Blake, M.P. Halsall, A.C. Ferrari, D.W. Boukhvalov, M.I. Katsnelson, A.K. Geim, et al., Control of graphene's properties by reversible hydrogenation: evidence for graphane, *Science* 323 (2009) 610.
- [66] L. Openov, A. Podlivaev, Spontaneous regeneration of an atomically sharp graphene/graphane interface under thermal disordering, *JETP Lett.* 90 (2009) 459.
- [67] M.J. Schmidt, D. Loss, Tunable edge magnetism at graphene/graphane interfaces, *Phys. Rev. B* 82 (2010) 085422.
- [68] S.-H. Cheng, K. Zou, F. Okino, H.R. Gutierrez, A. Gupta, N. Shen, P.C. Eklund, J.O. Sofo, J. Zhu, Reversible fluorination of graphene: evidence of a two-dimensional wide bandgap semiconductor, *Phys. Rev. B* 81 (2010) 205435.
- [69] R.R. Nair, W. Ren, R. Jalil, I. Riaz, V.G. Kravets, L. Britnell, P. Blake, F. Schedin, A.S. Mayorov, S. Yuan, et al., Fluorographene: a two-dimensional counterpart of teflon, *Small* 6 (2010) 2877.
- [70] J.T. Robinson, J.S. Burgess, C.E. Junkermeier, S.C. Badescu, T.L. Reinecke, F.K. Perkins, M.K. Zalalutdinov, J.W. Baldwin, J.C. Culbertson, P.E. Sheehan, et al., Properties of fluorinated graphene films, *Nano Lett.* 10 (2010) 3001.
- [71] F. Withers, M. Dubois, A.K. Savchenko, Electron properties of fluorinated single-layer graphene transistors, *Phys. Rev. B* 82 (2010) 073403.
- [72] H.J. Xiang, E.J. Kan, S.-H. Wei, X.G. Gong, M.-H. Whangbo, Thermodynamically stable single-side hydrogenated graphene, *Phys. Rev. B* 82 (2010) 165425.
- [73] E. Bekyarova, M.E. Itkis, P. Ramesh, C. Berger, M. Sprinkle, W.A. de Heer, R.C. Haddon, Chemical modification of epitaxial graphene: spontaneous grafting of aryl groups, *J. Amer. Chem. Soc.* 131 (2009) 1336.
- [74] X. Li, X. Wang, L. Zhang, S. Lee, H. Dai, Chemically derived, ultrasmooth graphene nanoribbon semiconductors, *Science* 319 (2008) 1229.
- [75] X. Jia, M. Hofmann, V. Meunier, B.G. Sumpter, J. Campos-Delgado, J.M. Romo-Herrera, H. Son, Y.-P. Hsieh, A. Reina, J. Kong, et al., Controlled formation of sharp zigzag and armchair edges in graphitic nanoribbons, *Science* 323 (2009) 1701.
- [76] M. Engelund, J.A. Fürst, A.P. Jauho, M. Brandbyge, Localized edge vibrations and edge reconstruction by Joule heating in graphene nanostructures, *Phys. Rev. Lett.* 104 (2010) 036807.

- [77] X. Wang, Y. Ouyang, X. Li, H. Wang, J. Guo, H. Dai, Room-temperature all-semiconducting sub-10-nm graphene nanoribbon field-effect transistors, *Phys. Rev. Lett.* 100 (2008) 206803.
- [78] L. Liao, J. Bai, R. Cheng, Y.-C. Lin, S. Jiang, Y. Huang, X. Duan, Top-gated graphene nanoribbon transistors with ultrathin high- k dielectrics, *Nano Lett.* (2010).
- [79] J.W. Bai, X.F. Duan, Y. Huang, Rational fabrication of graphene nanoribbons using a nanowire etch mask, *Nano Lett.* 9 (2009) 2083.
- [80] V. Barone, O. Hod, G.E. Scuseria, Electronic structure and stability of semiconducting graphene nanoribbons, *Nano Lett.* 6 (2006) 2748.
- [81] L. Brey, H. Fertig, Electronic states of graphene nanoribbons studied with the Dirac equation, *Phys. Rev. B* 73 (2006) 235411.
- [82] Y.-W. Son, M.L. Cohen, S.G. Louie, Half-metallic graphene nanoribbons, *Nature* 444 (2006) 347.
- [83] L. Pisani, J.A. Chan, B. Montanari, N.M. Harrison, Electronic structure and magnetic properties of graphitic ribbons, *Phys. Rev. B* 75 (2007) 064418.
- [84] L. Yang, C.-H. Park, Y.-W. Son, M.L. Cohen, S.G. Louie, Quasiparticle energies and band gaps in graphene nanoribbons, *Phys. Rev. Lett.* 99 (2007) 186801.
- [85] M. Zarea, N. Sandler, Electron–electron and spin–orbit interactions in armchair graphene ribbons, *Phys. Rev. Lett.* 99 (2007) 256804.
- [86] F. Sols, F. Guinea, A.H.C. Neto, Coulomb blockade in graphene nanoribbons, *Phys. Rev. Lett.* 99 (2007) 166803.
- [87] Y.-W. Son, M.L. Cohen, S.G. Louie, Energy gaps in graphene nanoribbons, *Phys. Rev. Lett.* 97 (2006) 216803.
- [88] A.V. Rozhkov, S. Savel'ev, F. Nori, Electronic properties of armchair graphene nanoribbons, *Phys. Rev. B* 79 (2009) 125420.
- [89] C.T. White, J. Li, D. Gunlycke, J.W. Mintmire, Hidden one-electron interactions in carbon nanotubes revealed in graphene nanostrips, *Nano Lett.* 7 (2007) 825.
- [90] D. Gunlycke, C.T. White, Tight-binding energy dispersions of armchair-edge graphene nanostrips, *Phys. Rev. B* 77 (2008) 115116.
- [91] M. Fujita, K. Wakabayashi, K. Nakada, K. Kusakabe, Peculiar localized state at zigzag graphite edge, *J. Phys. Soc. Japan* 65 (1996) 1920.
- [92] K. Kusakabe, M. Maruyama, Magnetic nanographite, *Phys. Rev. B* 67 (2003) 092406.
- [93] F. Cervantes-Sodi, G. Csanyi, S. Piscanec, A.C. Ferrari, Edge-functionalized and substitutionally doped graphene nanoribbons: electronic and spin properties, *Phys. Rev. B* 77 (2008) 165427.
- [94] O. Hod, V. Barone, G.E. Scuseria, Edge-functionalized and substitutionally doped graphene nanoribbons: electronic and spin properties, *Phys. Rev. B* 77 (2008) 035411.
- [95] E. Rudberg, P. Salek, Y. Luo, Nonlocal exchange interaction removes half-metallicity in graphene nanoribbons, *Nano Lett.* 7 (2007) 2211.
- [96] O. Hod, V. Barone, J.E. Peralta, G.E. Scuseria, Enhanced half-metallicity in edge-oxidized zigzag graphene nanoribbons, *Nano Lett.* 7 (2007) 2295.
- [97] S. Dutta, A.K. Manna, S.K. Pati, Intrinsic half-metallicity in modified graphene nanoribbons, *Phys. Rev. Lett.* 102 (2009) 096601.
- [98] G. Mahan, *Many-Particle Physics*, Kluwer Academic/Plenum Publishers, New York, 2000.
- [99] A.K. Singh, B.I. Yakobson, Electronics and magnetism of patterned graphene nanoroads, *Nano Lett.* 9 (2009) 1540.
- [100] V. Tozzini, V. Pellegrini, Electronic structure and Peierls instability in graphene nanoribbons sculpted in graphane, *Phys. Rev. B* 81 (2010) 113404.
- [101] H. Xiang, E. Kan, S.-H. Wei, M.-H. Whangbo, J. Yang, 'Narrow' graphene nanoribbons made easier by partial hydrogenation, *Nano Lett.* 9 (2009) 4025.
- [102] M.J. Schmidt, D. Loss, Edge states and enhanced spin–orbit interaction at graphene/graphane interfaces, *Phys. Rev. B* 81 (2010) 165439.
- [103] N. Peres, A. Neto, F. Guinea, Conductance quantization in mesoscopic graphane, *Phys. Rev. B* 73 (2006) 195411.
- [104] N.M.R. Peres, The transport properties of graphane, *J. Phys.: Condens. Matter* 21 (2009) 323201.
- [105] J. Tworzydło, B. Trauzettel, M. Titov, A. Rycerz, C.W.J. Beenakker, Sub-poissonian shot noise in graphane, *Phys. Rev. Lett.* 96 (2006) 246802.
- [106] F. Miao, S. Wijeratne, Y. Zhang, U.C. Coskun, W. Bao, C.N. Lau, Phase-coherent transport in graphane quantum billiards, *Science* 317 (2007) 1530.
- [107] D.A. Areshkin, D. Gunlycke, C.T. White, Ballistic transport in graphane nanostrips in the presence of disorder: importance of edge effects, *Nano Lett.* 7 (2007) 204.
- [108] M. Evaldsson, I.V. Zozoulenko, H. Xu, T. Heinzl, Edge-disorder-induced Anderson localization and conduction gap in graphene nanoribbons, *Phys. Rev. B* 78 (2008) 161407.
- [109] D. Gunlycke, D.A. Areshkin, C.T. White, Semiconducting graphene nanostrips with edge disorder, *Appl. Phys. Lett.* 90 (2007) 142104.
- [110] E.R. Mucciolo, A.H. Castro Neto, C.H. Lewenkopf, Conductance quantization and transport gaps in disordered graphene nanoribbons, *Phys. Rev. B* 79 (2009) 075407.
- [111] B. Biel, X. Blase, F. Triozon, S. Roche, Anomalous doping effects on charge transport in graphene nanoribbons, *Phys. Rev. Lett.* 102 (2009) 096803.
- [112] D. Gunlycke, J. Li, J.W. Mintmire, C.T. White, Altering low-bias transport in zigzag-edge graphene nanostrips with edge chemistry, *Appl. Phys. Lett.* 91 (2007) 112108.
- [113] F. Molitor, A. Jacobsen, C. Stampfer, J. Güttinger, T. Ihn, K. Ensslin, Transport gap in side-gated graphene constrictions, *Phys. Rev. B* 79 (2009) 075426.
- [114] C. Stampfer, J. Güttinger, S. Hellmueller, F. Molitor, K. Ensslin, T. Ihn, Energy gaps in etched graphene nanoribbons, *Phys. Rev. Lett.* 102 (2009) 056403.
- [115] K. Todd, H.T. Chou, S. Amasha, D. Goldhaber-Gordon, Quantum dot behavior in graphene nanoconstrictions, *Nano Lett.* 9 (2009) 416.
- [116] P. Gallagher, K. Todd, D. Goldhaber-Gordon, Disorder-induced gap behavior in graphene nanoribbons, *Phys. Rev. B* 81 (2010) 115409.
- [117] W.G. van der Wiel, S. De Franceschi, J.M. Elzerman, T. Fujisawa, S. Tarucha, L.P. Kouwenhoven, Electron transport through double quantum dots, *Rev. Modern Phys.* 75 (2003) 1.
- [118] S.M. Reimann, M. Manninen, Electronic structure of quantum dots, *Rev. Modern Phys.* 74 (2002) 1283.
- [119] P. Michler (Ed.), *Single Semiconductor Quantum Dots (NanoScience and Technology)*, Springer, Berlin, 2009.
- [120] I. Buluta, F. Nori, Quantum simulators, *Science* 326 (2009) 108.
- [121] I. Buluta, S. Ashhab, F. Nori, Natural and artificial atoms for quantum computation, <http://arxiv.org/abs/1002.1871>, 2010.
- [122] M. Ezawa, Metallic graphene nanodisks: electronic and magnetic properties, *Phys. Rev. B* 76 (2007) 245415.
- [123] J. Viana-Gomes, V.M. Pereira, N.M.R. Peres, Magnetism in strained graphene dots, *Phys. Rev. B* 80 (2009) 245436.
- [124] J. Fernandez-Rossier, J.J. Palacios, Magnetism in graphene nanoislands, *Phys. Rev. Lett.* 99 (2007) 177204.
- [125] C.L. Tang, W.H. Yan, Y.S. Zheng, G.S. Li, L.P. Li, Dirac equation description of the electronic states and magnetic properties of a square graphene quantum dot, *Nanotechnology* 19 (2008) 435401.
- [126] S. Bhowmick, V.B. Shenoy, Edge state magnetism of single layer graphene nanostructures, *J. Chem. Phys.* 128 (2008) 244717.
- [127] J. Akola, H.P. Heiskanen, M. Manninen, Edge-dependent selection rules in magic triangular graphene flakes, *Phys. Rev. B* 77 (2008) 193410.
- [128] H.P. Heiskanen, M. Manninen, J. Akola, Electronic structure of triangular, hexagonal and round graphene flakes near the Fermi level, *New J. Phys.* 10 (2008) 103015.
- [129] S.C. Kim, P.S. Park, S.R.E. Yang, States near Dirac points of a rectangular graphene dot in a magnetic field, *Phys. Rev. B* 81 (2010) 085432.
- [130] P. Potasz, A.D. Güçlü, P. Hawrylak, Zero-energy states in triangular and trapezoidal graphene structures, *Phys. Rev. B* 81 (2010) 033403.
- [131] M. Ezawa, Dirac fermions in a graphene nanodisk and a graphene corner: texture of vortices with an unusual winding number, *Phys. Rev. B* 81 (2010) 201402.
- [132] A.V. Rozhkov, F. Nori, Exact wave functions for an electron on a graphene triangular quantum dot, *Phys. Rev. B* 81 (2010) 155401.
- [133] M. Wimmer, A.R. Akhmerov, F. Guinea, Robustness of edge states in graphene quantum dots, *Phys. Rev. B* 82 (2010) 045409.
- [134] T.M.G. Mohiuddin, A. Lombardo, R.R. Nair, A. Bonetti, G. Savini, R. Jalil, N. Bonini, D.M. Basko, C. Galiotis, M. Marzari, et al., Uniaxial strain in graphene by Raman spectroscopy: G peak splitting, Grüneisen parameters, and sample orientation, *Phys. Rev. B* 79 (2009) 205433.
- [135] J.S. Bunch, Y. Yaish, M. Brink, K. Bolotin, P.L. McEuen, Coulomb oscillations and Hall effect in quasi-2D graphite quantum dots, *Nano Lett.* 5 (2005) 287.
- [136] L.A. Ponomarenko, F. Schedin, M.I. Katsnelson, R. Yang, E.W. Hill, K.S. Novoselov, A.K. Geim, Chaotic Dirac billiard in graphene quantum dots, *Science* 320 (2008) 356.
- [137] C. Stampfer, J. Güttinger, F. Molitor, D. Graf, T. Ihn, K. Ensslin, Tunable Coulomb blockade in nanostructured graphene, *Appl. Phys. Lett.* 92 (2008) 012102.
- [138] C. Stampfer, E. Schurtenberger, F. Molitor, J. Güttinger, T. Ihn, K. Ensslin, Tunable graphene single electron transistor, *Nano Lett.* 8 (2008) 2378.

- [139] J. Guttinger, C. Stampfer, S. Hellmüller, F. Molitor, T. Ihn, K. Ensslin, Charge detection in graphene quantum dots, *Appl. Phys. Lett.* 93 (2008) 212102.
- [140] F. Molitor, S. Droscher, J. Guttinger, A. Jacobsen, C. Stampfer, T. Ihn, K. Ensslin, Transport through graphene double dots, *Appl. Phys. Lett.* 94 (2009) 222107.
- [141] J. Guttinger, T. Frey, C. Stampfer, T. Ihn, K. Ensslin, Spin states in graphene quantum dots, *Phys. Rev. Lett.* 105 (2010) 116801.
- [142] M.I. Katsnelson, K.S. Novoselov, A.K. Geim, Chiral tunnelling and the Klein paradox in graphene, *Nat. Phys.* 2 (2006) 620.
- [143] N. Stander, B. Huard, D. Goldhaber-Gordon, Evidence for Klein tunneling in graphene p–n Junctions, *Phys. Rev. Lett.* 102 (2009) 026807.
- [144] H.Y. Chen, V. Apalkov, T. Chakraborty, Fock-Darwin states of Dirac electrons in graphene-based artificial atoms, *Phys. Rev. Lett.* 98 (2007) 186803.
- [145] A. Matulis, F.M. Peeters, Quasibound states of quantum dots in single and bilayer graphene, *Phys. Rev. B* 77 (2008) 115423.
- [146] P. Hewageegana, V. Apalkov, Electron localization in graphene quantum dots, *Phys. Rev. B* 77 (2008) 245426.
- [147] J.H. Bardarson, M. Titov, P.W. Brouwer, Electrostatic confinement of electrons in an integrable graphene quantum dot, *Phys. Rev. Lett.* 102 (2009) 226803.
- [148] G. Giavaras, P.A. Maksym, M. Roy, Magnetic field induced confinement–deconfinement transition in graphene quantum dots, *J. Phys.: Condens. Matter* 21 (2009) 102201.
- [149] P.A. Maksym, M. Roy, M.F. Craciun, S. Russo, M. Yamamoto, S. Tarucha, H. Aoki, Proposal for a magnetic field induced graphene dot, *J. Phys.: Conf. Ser.* 245 (2010) 012030.
- [150] A. De Martino, L. Dell'Anna, R. Egger, Magnetic confinement of Massless Dirac fermions in graphene, *Phys. Rev. Lett.* 98 (2007) 066802.
- [151] M.R. Masir, A. Matulis, F.M. Peeters, Quasibound states of Schrodinger and Dirac electrons in a magnetic quantum dot, *Phys. Rev. B* 79 (2009) 155451.
- [152] G. Giavaras, P.A. Maksym, M. Roy, Electron confinement in single layer graphene quantum dots: semiclassical approach, *Physica E* 42 (2010) 715.
- [153] P.S. Park, S.C. Kim, S.R.E. Yang, Electronic properties of a graphene antidot in magnetic fields, *J. Phys.: Condens. Matter* 22 (2010) 375302.
- [154] P.G. Silvestrov, K.B. Efetov, Quantum dots in graphene, *Phys. Rev. Lett.* 98 (2007) 016802.
- [155] B. Trauzettel, D.V. Bulaev, D. Loss, G. Burkard, Spin qubits in graphene quantum dots, *Nat. Phys.* 3 (2007) 192.
- [156] P. Recher, B. Trauzettel, Quantum dots and spin qubits in graphene, *Nanotechnology* 21 (2010) 302001.
- [157] X.L. Liu, J.B. Oostinga, A.F. Morpurgo, L.M.K. Vandersypen, Electrostatic confinement of electrons in graphene nanoribbons, *Phys. Rev. B* 80 (2009) 121407(R).
- [158] P. Recher, J. Nilsson, G. Burkard, B. Trauzettel, Bound states and magnetic field induced valley splitting in gate-tunable graphene quantum dots, *Phys. Rev. B* 79 (2009) 085407.
- [159] J.M. Pereira, P. Vasilopoulos, F.M. Peeters, Tunable quantum dots in bilayer graphene, *Nano Lett.* 7 (2007) 946.
- [160] G. Giavaras, F. Nori, Graphene quantum dots formed by a spatial modulation of the Dirac gap, *Appl. Phys. Lett.* 97 (2010) 243106.
- [161] G. Giavaras, F. Nori, Dirac gap-induced graphene quantum dot in an electrostatic potential, *Phys. Rev. B* (in press) <http://arxiv.org/abs/1102.3488>, 2011.
- [162] V.M. Pereira, A.H. Castro Neto, Strain engineering of graphene's electronic structure, *Phys. Rev. Lett.* 103 (2009) 046801.
- [163] A.K. Singh, E.S. Penev, B.I. Yakobson, Vacancy clusters in Graphene as quantum dots, *ACS Nano* 4 (2010) 3510.
- [164] S. Russo, J.B. Oostinga, D. Wehenkel, H.B. Heersche, S.S. Sobhani, L.M.K. Vandersypen, A.F. Morpurgo, Observation of Aharonov–Bohm conductance oscillations in a graphene ring, *Phys. Rev. B* 77 (2008) 085413.
- [165] P. Recher, B. Trauzettel, A. Rycerz, Y.M. Blanter, C.W.J. Beenakker, A.F. Morpurgo, Aharonov–Bohm effect and broken valley degeneracy in graphene rings, *Phys. Rev. B* 76 (2007) 235404.
- [166] M. Zarenia, J.M. Pereira, F.M. Peeters, G.A. Farias, Electrostatically confined quantum rings in bilayer graphene, *Nano Lett.* 9 (2009) 4088.
- [167] D.S.L. Abergel, V.M. Apalkov, T. Chakraborty, Interplay between valley polarization and electron–electron interaction in a graphene ring, *Phys. Rev. B* 78 (2008) 193405.
- [168] T. Echtermeyer, M. Lemme, M. Baus, B. Szafranek, A. Geim, H. Kurz, Nonvolatile switching in graphene field-effect devices, *Electron Device Lett., IEEE* 29 (2008) 952.
- [169] F. Traversi, V. Russo, R. Sordan, Integrated complementary graphene inverter, *Appl. Phys. Lett.* 94 (2009) 223312.
- [170] T. Cohen-Karni, Q. Qing, Q. Li, Y. Fang, C.M. Lieber, Graphene and nanowire transistors for cellular interfaces and electrical recording, *Nano Lett.* 10 (2010) 1098.
- [171] V.V. Cheianov, V.I. Fal'ko, Selective transmission of Dirac electrons and ballistic magnetoresistance of n–p junctions in graphene, *Phys. Rev. B* 74 (2006) 041403.
- [172] J. Cayssol, B. Huard, D. Goldhaber-Gordon, Contact resistance and shot noise in graphene transistors, *Phys. Rev. B* 79 (2009) 075428.
- [173] L.M. Zhang, M.M. Fogler, Nonlinear screening and ballistic transport in a graphene p–n junction, *Phys. Rev. Lett.* 100 (2008) 116804.
- [174] M.M. Fogler, D.S. Novikov, L.I. Glazman, B.I. Shklovskii, Effect of disorder on a graphene p–n junction, *Phys. Rev. B* 77 (2008) 075420.
- [175] M. Lemme, T. Echtermeyer, M. Baus, H. Kurz, A graphene field-effect device, *IEEE Electron Device Lett.* 28 (2007) 282.
- [176] B. Huard, J.A. Sulpizio, N. Stander, K. Todd, B. Yang, D. Goldhaber-Gordon, Transport measurements across a tunable potential barrier in graphene, *Phys. Rev. Lett.* 98 (2007) 236803.
- [177] B. Oezylmaz, P. Jarillo-Herrero, D. Efetov, D.A. Abanin, L.S. Levitov, P. Kim, Electronic transport and quantum hall effect in bipolar graphene p–n–p junctions, *Phys. Rev. Lett.* 99 (2007) 166804.
- [178] J.R. Williams, L. DiCarlo, C.M. Marcus, Quantum hall effect in a gate-controlled p–n junction of graphene, *Science* 317 (2007) 638.
- [179] V.V. Cheianov, V. Fal'ko, B.L. Altshuler, The focusing of electron flow and a Veselago lens in graphene p–n junctions, *Science* 315 (2007) 1252.
- [180] J. Cserti, A. Pályi, C. Péterfalvi, Caustics due to a negative refractive index in circular graphene p–n Junctions, *Phys. Rev. Lett.* 99 (2007) 246801.
- [181] B. Huard, N. Stander, J.A. Sulpizio, D. Goldhaber-Gordon, Evidence of the role of contacts on the observed electron–hole asymmetry in graphene, *Phys. Rev. B* 78 (2008) 121402.
- [182] Y.M. Blanter, I. Martin, Transport through normal–metal–graphene contacts, *Phys. Rev. B* 76 (2007) 155433.
- [183] J.P. Robinson, H. Schomerus, Electronic transport in normal–conductor/graphene/normal–conductor junctions and conditions for insulating behavior at a finite charge–carrier density, *Phys. Rev. B* 76 (2007) 115430.
- [184] R. Golizadeh-Mojarad, S. Datta, Effect of contact induced states on minimum conductivity in graphene, *Phys. Rev. B* 79 (2009) 085410.
- [185] G. Giovannetti, P.A. Khomyakov, G. Brocks, V.M. Karpan, J. van den Brink, P.J. Kelly, Doping graphene with metal contacts, *Phys. Rev. Lett.* 101 (2008) 026803.
- [186] P.A. Khomyakov, G. Giovannetti, P.C. Rusu, G. Brocks, J. van den Brink, P.J. Kelly, First-principles study of the interaction and charge transfer between graphene and metals, *Phys. Rev. B* 79 (2009) 195425.
- [187] E. Rossi, J.H. Bardarson, P.W. Brouwer, S. Das Sarma, Signatures of Klein tunneling in disordered graphene p–n–p junctions, *Phys. Rev. B* 81 (2010) 121408.
- [188] Y.P. Bliokh, V. Freilikher, S. Savel'ev, F. Nori, Transport and localization in periodic and disordered graphene superlattices, *Phys. Rev. B* 79 (2009) 075123.
- [189] D.P. Arovas, L. Brey, H.A. Fertig, E.-A. Kim, K. Ziegler, Dirac spectrum in piecewise constant one-dimensional potentials, <http://arxiv.org/abs/1002.3655>, 2010.
- [190] A.F. Young, P. Kim, Quantum interference and Klein tunnelling in graphene heterojunctions, *Nat. Phys.* 5 (2009) 222.
- [191] J.J. Velasco, G. Liu, W. Bao, C.N. Lau, Electrical transport in high-quality graphene pnp junctions, *New J. Phys.* 11 (2009) 095008.
- [192] R.V. Gorbachev, A.S. Mayorov, A.K. Savchenko, D.W. Horsell, F. Guinea, Conductance of p–n–p structures with “Air-Bridge top gates”, *Nano Lett.* 8 (2008) 1995.
- [193] V.G. Veselago, The electrodynamics of substances with simultaneously negative values of ϵ and μ , *Sov. Phys. Usp.* 10 (1967) 509.
- [194] J.B. Pendry, Negative refraction makes a perfect lens, *Phys. Rev. Lett.* 85 (2000) 3966.
- [195] A.N. Lagarkov, V.N. Kissel, Near-perfect imaging in a focusing system based on a left-handed-material plate, *Phys. Rev. Lett.* 92 (2004) 077401.

- [196] A.N. Lagarkov, A.K. Sarychev, V.N. Kissel, G. Tartakovskiy, Superresolution and enhancement in metamaterials, *Phys. Usp.* 52 (2009) 959.
- [197] K.Y. Bliokh, Y.P. Bliokh, V. Freilikher, S. Savel'ev, F. Nori, Colloquium: unusual resonators: plasmonics, metamaterials, and random media, *Rev. Modern Phys.* 80 (2008) 1201.
- [198] A.V. Kats, S. Savel'ev, V.A. Yampol'skii, F. Nori, Left-handed interfaces for electromagnetic surface waves, *Phys. Rev. Lett.* 98 (2007) 073901.
- [199] J.R. Williams, T. Low, M.S. Lundstrom, C.M. Marcus, Gate-controlled guiding of electrons in graphene, <http://arxiv.org/abs/1008.3704>, 2010.
- [200] V.A. Yampol'skii, S. Savel'ev, F. Nori, Voltage-driven quantum oscillations in graphene, *New J. Phys.* 10 (2008) 053024.
- [201] J.-A. Yan, L. Xian, M.Y. Chou, Structural and electronic properties of oxidized graphene, *Phys. Rev. Lett.* 103 (2009) 086802.
- [202] K. Novoselov, Beyond the wonder material, *Phys. World* 22 (2009) 27.
- [203] F. Guinea, M.I. Katsnelson, A.K. Geim, Energy gaps and a zero-field quantum Hall effect in graphene by strain engineering, *Nat. Phys.* 6 (2010) 30.
- [204] V. Pereira, A.H. Castro Neto, H. Liang, L. Mahadevan, Geometry, mechanics and electronics of singular structures and wrinkles in graphene, <http://arxiv.org/abs/1004.5384>, 2010.
- [205] V.M. Pereira, A.H. Castro Neto, N.M.R. Peres, Tight-binding approach to uniaxial strain in graphene, *Phys. Rev. B* 80 (2009) 045401.
- [206] N. Levy, S.A. Burke, K.L. Meaker, M. Panlasigui, A. Zettl, F. Guinea, A.H.C. Neto, M.F. Crommie, Strain-induced pseudo-magnetic fields greater than 300 tesla in graphene nanobubbles, *Science* 329 (2010) 544.
- [207] N. Peres, The transport properties of graphene, *J. Phys.: Condens. Matter* 21 (2009) 323201.
- [208] M. Titov, Impurity-assisted tunneling in graphene, *Europhys. Lett.* 79 (2007) 17004.
- [209] A.K. Geim, Graphene: status and prospects, *Science* 324 (2009) 1530.
- [210] S. Ghosh, M. Sharma, Electron optics with magnetic vector potential barriers in graphene, *J. Phys.: Condens. Matter* 21 (2009) 292204.
- [211] A.R. Akhmerov, J.H. Bardarson, A. Rycerz, C.W.J. Beenakker, Theory of the valley-valve effect in graphene nanoribbons, *Phys. Rev. B* 77 (2008) 205416.
- [212] A. De Martino, L. Dell'Anna, R. Egger, Magnetic barriers and confinement of Dirac–Weyl quasiparticles in graphene, *Solid State Commun.* 144 (2007) 547.
- [213] L. Dell'Anna, A. De Martino, Multiple magnetic barriers in graphene, *Phys. Rev. B* 79 (2009) 045420.
- [214] R. Masir, P. Vasilopoulos, A. Matulis, F.M. Peeters, Direction-dependent tunneling through nanostructured magnetic barriers in graphene, *Phys. Rev. B* 77 (2008) 235443.
- [215] J.E. Müller, Effect of a nonuniform magnetic field on a two-dimensional electron gas in the ballistic regime, *Phys. Rev. Lett.* 68 (1992) 385.
- [216] S. Park, H.-S. Sim, Magnetic edge states in graphene in nonuniform magnetic fields, *Phys. Rev. B* 77 (2008) 075433.
- [217] L. Oroszlány, P. Rakyta, A. Kormányos, C.J. Lambert, J. Cserti, Theory of snake states in graphene, *Phys. Rev. B* 77 (2008) 081403.
- [218] T.K. Ghosh, A. De Martino, W. Häusler, L. Dell'Anna, R. Egger, Conductance quantization and snake states in graphene magnetic waveguides, *Phys. Rev. B* 77 (2008) 081404.
- [219] Y.P. Bliokh, V. Freilikher, F. Nori, Tunable electronic transport and unidirectional quantum wires in graphene subjected to electric and magnetic fields, *Phys. Rev. B* 81 (2010) 075410.
- [220] R. Pollet, H. Amara, Spin-unrestricted calculations of bare-edged nanographenes using DFT and many-body perturbation theory, *J. Chem. Theory Comput.* 5 (2009) 1719.